

**OPTIMIZATION OF OXIDE ADDITIVES IN
BORON CARBIDE POWDERS USING
PRECIPITATION METHOD**

**A Thesis Submitted to
the Graduate School of Engineering and Sciences of
İzmir Institute of Technology
in Partial Fulfillment of the Requirements for the Degree of**

MASTER OF SCIENCE

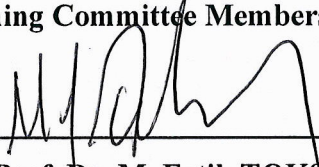
in Mechanical Engineering

**by
Caner ELÇİ**

**December 2019
İZMİR**

We approve the thesis of **Caner ELÇİ**

Examining Committee Members:



Assist. Prof. Dr. M. Fatih TOKSOY

Department of Mechanical Engineering, İzmir Institute of Technology



Assoc. Prof. Dr. Sinan KANDEMİR

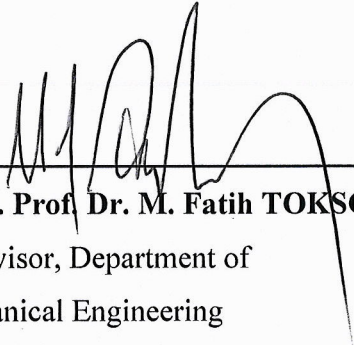
Department of Mechanical Engineering, İzmir Institute of Technology



Assoc. Prof. Dr. Mehmet Faruk EBEOĞLUGİL

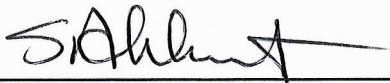
Department of Metallurgical and Materials Engineering, Dokuz Eylül University

19 December 2019



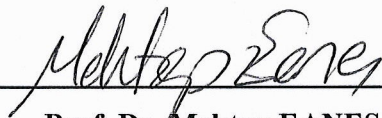
Assist. Prof. Dr. M. Fatih TOKSOY

Supervisor, Department of
Mechanical Engineering
İzmir Institute of Technology



Prof. Dr. Sedat AKKURT

Head of the Department of
Mechanical Engineering



Prof. Dr. Mehtap EANES

Dean of the Graduate School of
Engineering and Sciences

ACKNOWLEDGMENTS

First of all, I would like to offer my special thanks to Assist. Prof. Dr. M. Fatih TOKSOY for his valuable suggestions and comments. It was a pleasure for me to study under his guidance and supervising. I also thank to all faculty members who helped me during my experiments. I am grateful for the efforts of the İYTE MAM and BIYOMER members.

My deepest gratitude goes to my family, Yaşar ELÇİ and Zehra ELÇİ, for supporting me and always telling me to finish what I started. It would be a very hard journey without their encouragement.

Finally, I would like to thank to very special person, my wife Beste ELÇİ, for her continuous support during the process.

ABSTRACT

OPTIMIZATION OF OXIDE ADDITIVES IN BORON CARBIDE POWDERS USING PRECIPITATION METHOD

This study aims to precipitate oxides to boron carbide powders to achieve homogeneous dispersion of additive which is essential for sintering. Fine boron carbide powders were suspended in distilled water, then nitrate salts were solved in alcohol. Solved nitrate salts were fed to mixture in high pH levels. Mixing stage of the precipitation was done with both magnetic stirrer and ultrasonic treatment to investigate the effect of the mixing method. After the precipitation, synthesized powders were calcined under various atmospheres to eliminate the inorganic residues from the precipitation process. The examination of the XRD graphs showed that the calcination atmosphere is important for the oxide layer of the boron carbide powders. Inert atmosphere restrained the formation of the boron oxide layer due to the lack of oxygen. Methanol washing also eliminated the boron oxide layer. According to the zeta potential analysis, surface characteristics were obtained better when the ultrasonic treatment was applied during the precipitation. Ultrasonic treatment increased the dispersion of the additives between the particles during the suspension stage of the precipitation. Calcination time also affected the dispersion of the yttrium oxide at the sintered compacts when the SEM images were observed. When the calcination time increased, dispersion of the yttria was getting more agglomerated.

ÖZET

ÇÖKELTME YÖNTEMİ KULLANILARAK BOR KARBÜR TOZLARININ İÇİNDEKİ OKSİT KATKILARININ OPTİMİZASYONU

Bu çalışmada, bor karbür tozları tane sınırları arasında sıvı faz sinterlemesi sayesinde homojen dağılım elde etmek amacıyla oksit sinterleme katkıları kullanılarak çökeltme yöntemi ile katkılanmıştır. Çökeltme yöntemi sırasında mikro ölçekli bor karbür tozları sıvı içerisinde oksit katkıların nitrat tuzları ile askıda bırakılmıştır. Bu yöntemin karıştırma aşaması hem manyetik karıştırıcı ile hem de ultrasonik karıştırıcı ile gerçekleştirilmiştir. Çökeltmeden sonra elde edilen tozlar farklı atmosferlerde kalsine edilecek inorganik kalıntıların giderilmesi amaçlanmıştır. XRD grafikleri gözleendiğinde kalsinasyon atmosferinin bor karbür üzerindeki oksit tabakası için önemli olduğu görülmüştür. Asal gazdan oluşan atmosferdeki oksijen azlığı sebebiyle boron oksit tabakası gözlenmemiştir. Metanol ile yıkama işlemi de ayrıca oksit tabakasını gidermektedir. Zeta potansiyel analizine göre, çökeltme sırasındaki ultrasonik karıştırma işlemi daha iyi bir yüzey karakteristiği göstermiştir. Ultrasonik karıştırma askıda kalma esnasında parçacıklar arasındaki dağılımın daha homojen olmasını sağlamıştır. Ayrıca SEM görüntülerine bakıldığında kalsinasyon süresi sinterlenen peletlerdeki itriyum oksit dağılımını da etkilemektedir. Kalsinasyon süresi arttıkça itriyum oksidin bor karbür içerisinde öbeklendiği görülmüştür.

TABLE OF CONTENTS

LIST OF FIGURES	viii
LIST OF TABLES.....	xii
CHAPTER 1. INTRODUCTION	1
CHAPTER 2. BORON CARBIDE AND ITS ADDITIVES.....	2
2.1. Boron Carbide	2
2.1.1. Sintering of Boron Carbide	3
2.1.2. Sintering Methods	4
2.1.2.1. Pressureless Sintering	5
2.1.2.2. Hot Pressing	5
2.1.2.3. Spark Plasma Sintering	6
2.1.3. Solid State Sintering.....	6
2.1.4. Liquid Phase Sintering	7
2.2. Literature Survey about the Effects of Additives on B ₄ C	8
CHAPTER 3. MATERIALS AND EXPERIMENTAL PROCEDURES	11
3.1. Selected Additives and Their Ratio	11
3.2. Precipitation Method as an Improved Processing	12
3.2.1. Procedures of the Precipitation	13
3.2.2. Raw Materials	15
3.2.3. Initial pH Studies.....	16
3.2.4. Calculations of the Precipitation Method.....	17
3.3. Characterization Techniques	18

3.3.1. Zeta Potential	18
3.3.2. X-Ray Diffractometry	19
3.3.3. Sintering, Cutting, Grinding, Polishing.....	20
3.3.4. Scanning Electron Microscopy	23
3.3.5. Porosity Analysis via ImageJ Software.....	24
CHAPTER 4. RESULTS AND DISCUSSION.....	25
4.1. Initial Studies.....	25
4.2. Precipitation Studies of Boron Carbide.....	28
4.2.1. Powder Analysis of Precipitated B ₄ C Powders with the Oxide Additives Calcined under Ambient Atmosphere.....	28
4.2.2. Powder Analysis of Precipitated B ₄ C Powders with the Oxide Additives Synthesized with 2 Burettes Calcined under Ambient Atmosphere.....	33
4.2.3. Powder Analysis of Precipitated B ₄ C Powders with the Oxide Additives Calcined under Ar Atmosphere.....	35
4.2.4. Calcination Process under Protective Atmosphere	38
4.2.5. Ultrasonication Improvement for Optimized Precipitation.....	39
4.2.6. Comparison of the XRD Graphs of Powders.....	40
4.3. Sintering Studies.....	42
4.3.1. Effect of Precipitation Compared to Commercial Boron Carbide .	42
4.3.2. Effect of Calcination Time on Sintering	45
4.3.3. Sintered Sample of Milled Powders.....	52
CHAPTER 5. CONCLUSIONS	55
REFERENCES	57

LIST OF FIGURES

<u>Figure</u>	<u>Page</u>
Figure 1. Crystal structure of Boron Carbide	3
Figure 2. Schematic of hot pressing	5
Figure 3. Schematic of spark plasma sintering	6
Figure 4. Schematic of solid-state sintering	7
Figure 5. Schematic of the liquid phase sintering	7
Figure 6. Wetting behavior of the liquid	8
Figure 7. Phase diagram of $Al_2O_3 - Y_2O_3$	11
Figure 8. Example of the heterogeneous distribution of the additives and their interphases	12
Figure 9. Synthesized powders via the traditional milling method (left) and precipitation method (right).....	13
Figure 10. Procedures of the synthesizing of B_4C via the precipitation method	14
Figure 11. Zetasizer Nano device	18
Figure 12. X-Ray Diffraction device	19
Figure 13. High temperature furnace	20
Figure 14. Grinder-Polisher device.....	21
Figure 15. SEM device	23
Figure 16. Titration curves of the raw materials.....	25
Figure 17. XRD graph of the unprocessed B_4C	26
Figure 18. Zeta Potential graph of the B_4C	27
Figure 19. SEM image of the commercial boron carbide particles at high magnification	27
Figure 20. XRD graph of the precipitated B_4C powders with the additives of 3% $Al_2O_3 + 2\% Y_2O_3$	28
Figure 21. Zeta potential graph of the precipitated B_4C powders with the additives of 3% $Al_2O_3 + 2\% Y_2O_3$	29
Figure 22. SEM (secondary electron mode) image of the precipitated B_4C powders with the additives of 3% $Al_2O_3 + 2\% Y_2O_3$ at high magnification.....	30
Figure 23. SEM (backscatter electron mode) image of the precipitated B_4C powders with the additives of 3% $Al_2O_3 + 2\% Y_2O_3$ at low magnification.....	30

<u>Figure</u>	<u>Page</u>
Figure 24. XRD graph of the precipitated B ₄ C powders with the additives of 6% Al ₂ O ₃ + 4% Y ₂ O ₃	31
Figure 25. Zeta potential graph of the precipitated B ₄ C powders with the additives of 6% Al ₂ O ₃ + 4% Y ₂ O ₃	32
Figure 26. SEM (secondary electron mode) image of the precipitated B ₄ C powders with the additives of 6% Al ₂ O ₃ + 4% Y ₂ O ₃ at high magnification.....	32
Figure 27. SEM (backscatter electron mode) image of the precipitated B ₄ C powders with the additives of 6% Al ₂ O ₃ + 4% Y ₂ O ₃ at low magnification.....	33
Figure 28. XRD graph of the precipitated B ₄ C powders with the additives of 3% Al ₂ O ₃ + 2% Y ₂ O ₃ (Precipitated with 2 burettes)	34
Figure 29. Zeta potential graph of the precipitated B ₄ C powders with the additives of 3% Al ₂ O ₃ + 2% Y ₂ O ₃ (Precipitated with 2 burettes).....	35
Figure 30. XRD graph of the precipitated B ₄ C powders with the additives of 3% Al ₂ O ₃ + 2% Y ₂ O ₃ (Calcined under Ar atmosphere)	36
Figure 31. Zeta potential graph of the precipitated B ₄ C powders with the additives of 3% Al ₂ O ₃ + 2% Y ₂ O ₃ (Calcined under Ar atmosphere).....	37
Figure 32. SEM (backscatter electron mode) image of the precipitated B ₄ C powders with the additives of 3% Al ₂ O ₃ + 2% Y ₂ O ₃ at a) low, b) high magnification (Calcined under Ar atmosphere).....	37
Figure 33. Zeta potential graph of the precipitated B ₄ C powders with the additives of 3% Al ₂ O ₃ + 2% Y ₂ O ₃ (Calcined under Ar atmosphere for 1-3-5 hours at 500 °C)	38
Figure 34. Zeta potential graph of the precipitated B ₄ C powders with the additives of 3% Al ₂ O ₃ + 2% Y ₂ O ₃ and 6% Al ₂ O ₃ + 4% Y ₂ O ₃ (Calcined under Ar atmosphere for 1 hour, mixed with ultrasonication method).....	39
Figure 35. SEM (backscatter electron mode) image of the a) precipitated, b) milled B ₄ C Powders with the additives of 3% Al ₂ O ₃ + 2% Y ₂ O ₃	40
Figure 36. Stacked XRD graph of the precipitated B ₄ C powders with the additives of 3% Al ₂ O ₃ + 2% Y ₂ O ₃ and 6% Al ₂ O ₃ + 4% Y ₂ O ₃	41
Figure 37. Stacked XRD graph of the precipitated B ₄ C powders with the additives of 3% Al ₂ O ₃ + 2% Y ₂ O ₃	42

<u>Figure</u>	<u>Page</u>
Figure 38. SEM (backscatter electron mode) image of the commercial B ₄ C compact at a) low, b) high magnification.....	43
Figure 39. SEM (secondary electron mode) image of the commercial B ₄ C compact at a) low, b) high magnification.....	43
Figure 40. Elemental mapping images of the precipitated B ₄ C Powders with the Oxide Additives Calcined under Ambient Atmosphere	44
Figure 41. SEM (backscatter electron mode) image of the precipitated B ₄ C Powders with the Oxide Additives Calcined under Ambient Atmosphere at a) low, b) high magnification.....	44
Figure 42. SEM (secondary electron mode) image of the precipitated B ₄ C Powders with the Oxide Additives Calcined under Ambient Atmosphere at a) low, b) high magnification.....	45
Figure 43. SEM (backscatter electron mode) image of the precipitated B ₄ C Powders with the Oxide Additives Calcined under Ar Atmosphere for 1 Hour at a) low, b) high magnification.....	46
Figure 44. Elemental mapping images of the precipitated B ₄ C Powders with the Oxide Additives Calcined under Ar Atmosphere for 1 Hour	46
Figure 45. SEM (secondary electron mode) image of the precipitated B ₄ C Powders with the Oxide Additives Calcined under Ar Atmosphere for 1 Hour at a) low, b) high magnification.....	46
Figure 46. SEM (backscatter electron mode) image of the precipitated B ₄ C Powders with the Oxide Additives Calcined under Ar Atmosphere for 3 Hours at a) low, b) high magnification.....	47
Figure 47. Elemental mapping images of the precipitated B ₄ C Powders with the Oxide Additives Calcined under Ar Atmosphere for 3 Hours.....	47
Figure 48. SEM (secondary electron mode) image of the precipitated B ₄ C Powders with the Oxide Additives Calcined under Ar Atmosphere for 3 Hours at a) low, b) high magnification.....	48
Figure 49. SEM (backscatter electron mode) image of the precipitated B ₄ C Powders with the Oxide Additives Calcined under Ar Atmosphere for 5 Hours at a) low, b) high magnification.....	48

<u>Figure</u>	<u>Page</u>
Figure 50. Elemental mapping images of the precipitated B ₄ C Powders with the Oxide Additives Calcined under Ar Atmosphere for 5 Hours.....	49
Figure 51. SEM (secondary electron mode) image of the precipitated B ₄ C Powders with the Oxide Additives Calcined under Ar Atmosphere for 5 Hours at a) low, b) high magnification.....	49
Figure 52. EDS maps of the yttrium in the precipitated and sintered B ₄ C powders with the additives of 3% Al ₂ O ₃ + 2% Y ₂ O ₃ (a) Calcined for 1 hour, b) Calcined for 3 hours, c) Calcined for 5 hours)	50
Figure 53. Elemental mapping images of the precipitated B ₄ C Powders with the Oxide Additives Calcined under Ar Atmosphere at 1000x magnification....	50
Figure 54. EDS graphs of the precipitated and sintered B ₄ C powders with the additives of 3% Al ₂ O ₃ + 2% Y ₂ O ₃ , a) Spectrum 6, b) Spectrum 7.....	51
Figure 55. SEM (backscatter electron mode) images of the milled B ₄ C Powders with the Oxide Additives at a) low, b) high magnification	53
Figure 56. Elemental mapping images of the milled B ₄ C Powders with the Oxide Additives at 2500x magnification.....	53

LIST OF TABLES

<u>Table</u>	<u>Page</u>
Table 1. Effects of the sintering additives on B ₄ C.....	10
Table 2. Comparison of the porosities of commercial, milled and precipitated boron carbide powders.....	54

CHAPTER 1

INTRODUCTION

Carbide ceramics are important materials because of their low densities, high hardness and high elastic modulus. Boron carbide is also an important ceramic material because of the desired characteristics such as high hardness and high melting point. While the boron carbide is useful for different scenarios such as armor plating, neutron absorber or nozzles, its production is not as easy as most of the metals.

Powder metallurgy method which is called as sintering is needed for producing boron carbide products. Sintering includes a heating cycle for bonding the particles together as a solid block and sintering of the boron carbide is not easy because of the high melting point of the material. Sintering additives are the main factor for both keeping characteristic properties stable and decreasing the sintering temperature of the boron carbide.

While the conventional method is mixing the sintering additives and the ceramic powder mechanically, precipitation method offers more homogeneous dispersion of the additives with the help of chemical processes. Better dispersion leads to better mechanical properties while the sintering temperature is getting lower.

The main purpose of this study is advancing the dispersion of the sintering additives through the precipitation method while the powders are kept oxide-free and coated with enough additives.

CHAPTER 2

BORON CARBIDE AND ITS ADDITIVES

General background information about boron carbide such as the general properties, literature survey about pressureless sintering of B₄C, sintering methods and sintering types are explained.

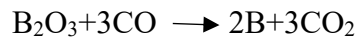
2.1. Boron Carbide

Boron carbide has an important place among the other non-metallic hard materials as alumina, silica, silicon nitride and diamond. It was firstly discovered in 1858, then, in 1883 by Joly and in 1894 by Moissan. Even if it was discovered at the late 19th century, its 4:1 stoichiometric ratio was identified in 1934 by Ridgway [1].

Boron carbide is a ceramic material which has covalent bonds at its crystal structure. It is also known as the third hardest material after cubic boron nitride and diamond [1]. B₄C has a relatively low density than most of the engineering materials (2,52 g/cm³), high Young's Modulus (450-470 GPa) and fracture toughness (450-470 MPa.m^{1/2}). It has a good nuclear property as a high neutron absorption cross section. Beside the advantages, it has a high melting point (2450 °C) and needs a high sintering temperature for >95% relative densities [2]. It is hard to densify because of the low self-diffusion coefficient, low plasticity and high resistance to grain boundary sliding [4]. B₄C has a limited moldability of the final products due to the production methods [5].

Most common synthesis method of the boron carbide is the carbothermic reduction of the boric acid. Boron oxide and water are obtained as a result of the heated boric acid. Boron oxide and carbon monoxide react and boron and carbon dioxide occur as a result of the reaction. This reaction is feasible when the temperature is higher than 1400 C. Electric arc furnace, Acheson type furnace and tubular furnace are the main furnace types to synthesize boron carbide with carbothermic reaction. Chemical reactions of the carbothermic reduction are demonstrated below [2].





Boron carbide has a complex crystal structure which can be proven by the nuclear magnetic resonance, IR absorption spectroscopy and XRD analysis. Even though the chemical formula of the boron carbide is known as B_4C because of its stoichiometric ratio, the ideal formula is B_{12}C_3 . It has a rhombohedral crystal structure and rhombohedral unit cell of the boron carbide consists of 15 atoms. Early studies show that the rhombohedral geometry occurred by the 12 boron atoms of icosahedras at the corner of the unit cell and each icosahedras bonded with covalent bonds. As seen in Figure 1, recent studies claimed that the crystal structure of the boron carbide consists C-B-C chain and icosahedras with 11 boron and a carbon atom [1,2,3].

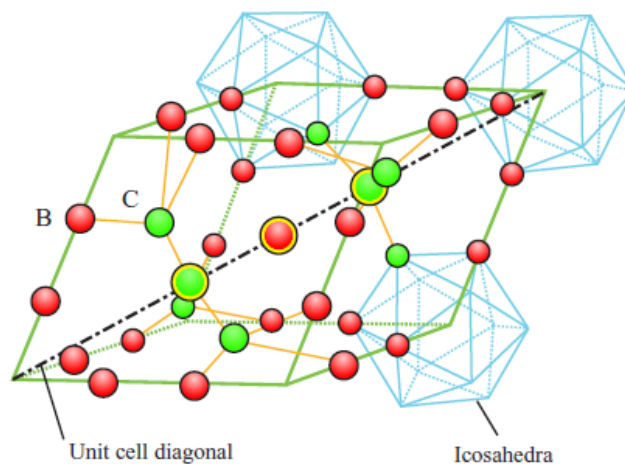


Figure 1. Crystal structure of Boron Carbide [3]

2.1.1. Sintering of Boron Carbide

Powder metallurgy is the main production method to produce boron carbide products. Due to the high melting point of B_4C , melting and casting methods are not convenient to produce desired components. In order to produce boron carbide products, sintering method is the only option to manufacture at the desired geometries. Because of the low self-diffusion coefficient, low plasticity and high resistance to grain boundary sliding, it is hard to apply pressureless sintering to the B_4C [4]. Grain boundary diffusion,

bulk diffusion, shrinkage, capillarity force, void growth and densification are the main micro-level mechanisms of the sintering [6].

Before the sintering, powders need to be formed in a mold with the certain pressure, which is called as a powder compaction. After the compaction, powders are ready to sinter at the furnace.

There are three main stages of the sintering.

- Neck Growth: When the powders are heated externally, neck growth occurs between the particles. There are internal micro-level normal and tangential stresses at the contact points of the particles. Bonding between particles are weak [6].
- Densification and Grain Growth: Necks between the particles intersect with each other. Capillary and diffusion mechanisms increase the necking and the density of the material. As a result of these mechanisms, porosity decreases [6].
- Closed Pore Stage: After the simultaneous necking, pores are decreased and isolated from the environment. Recrystallization occurs at the final stage of the sintering. For the ceramics, recrystallization takes a few hours in contrary to the metals. Relative density does not change at the final stage of the sintering [6].

All sintering methods need common parameters as micron sized powders (~1 micron), high temperatures, sintering additives or external pressure to obtain relative density higher than 90%. When the sintering aids are used, required sintering temperature, relative density and the mechanical properties of final product change. Even though the actual behavior of the sintering additive decreases the mechanical properties of the final product at the same relative density with the pure B_4C , mechanical properties of the material with sintering additive are higher than the pure B_4C due to the low sintering temperatures and low relative density of pure B_4C [8].

2.1.2. Sintering Methods

There are three methods of sintering B_4C .

Sintering Methods of B_4C without additives:

- Pressureless Sintering
- Hot Pressing
- Spark Plasma Sintering

2.1.2.1. Pressureless Sintering

Pressureless sintering is the hardest method to sinter the B_4C because of the lack of the external pressure. Very high temperatures ($\sim 2200\text{ }^\circ\text{C}$), long sintering times and micron sized powders are needed to sinter the B_4C . The sintering additives have to be used to achieve high densities, good mechanical properties and low sintering temperatures [8]. While the pressureless sintering is mainly established on solid-state sintering, sintering additives activate the liquid phase sintering with the presence of the liquid phases and secondary phases of the additives at the sintering temperature [2,9]. Most complex product shapes can be obtained with the pressureless sintering among the other sintering methods [7].

2.1.2.2. Hot Pressing

Hot pressing method has a uniaxial external pressure during the sintering as an additional parameter to the pressureless sintering. High temperatures ($\sim 2000\text{ }^\circ\text{C}$), relatively short sintering times than pressureless sintering, micron sized powders and external pressure are the main parameters to sinter the B_4C . Sintering additives affect the sintering parameters as same as the pressureless sintering. Due to the conventional molds, most of the components produced from the hot press is in cylindrical shape. Because the heating elements are placed around the mold and it prevents the geometry of the mold other than cylindrical [10].

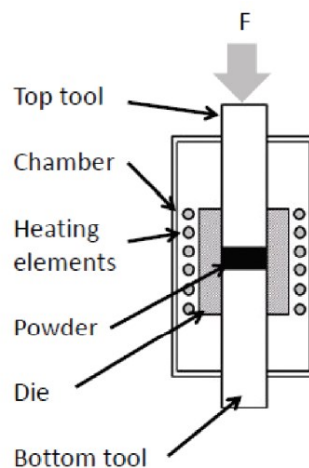


Figure 2. Schematic of hot pressing [10]

2.1.2.3. Spark Plasma Sintering

Spark plasma sintering method is the easiest way to sinter the B_4C . Lower temperatures (1800-1900 °C) than the temperatures of the hot-pressing method are necessary to sinter B_4C in spark plasma sintering. Although it has a uniaxial external pressure like hot pressing, it generates Joule heating inside the particles with the help of the pulsed current. Extremely high heating rates (up to 100-300 C/min) and very low dwell times (5-10 minutes) can be achieved in addition to fine grains and high densification [12]. Like the hot pressing, moldability of the material is very limited due to the geometric limitations of the graphite die.

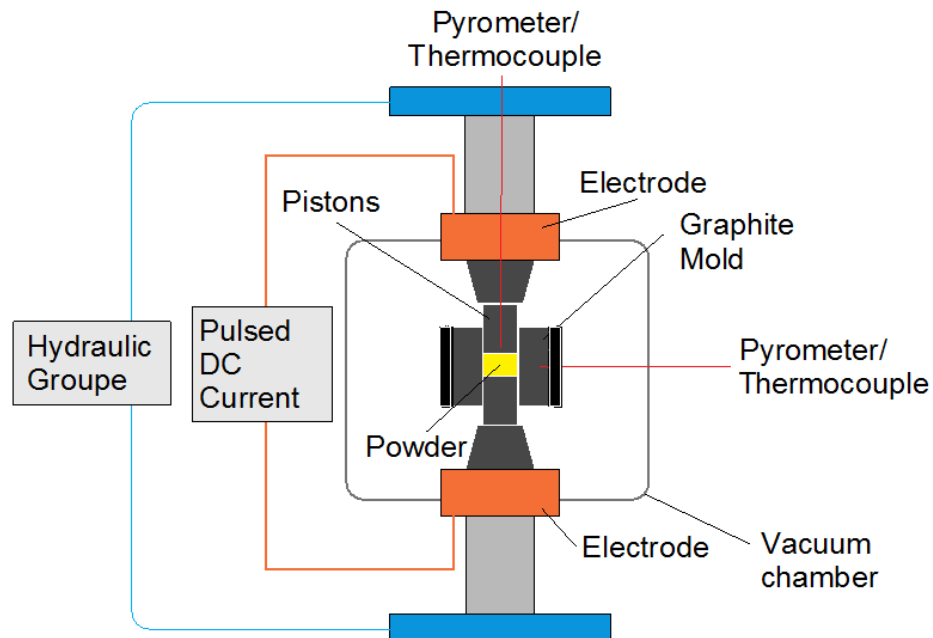


Figure 3. Schematic of spark plasma sintering [11]

2.1.3. Solid State Sintering

As discussed in the section 2.1.1, solid state sintering has 3 main stages as neck growth, densification and grain growth and close pore stage. After the necking and densification, while the pores at the grain boundaries can be eliminated with the grain boundary diffusion mechanism, fully eliminated pores inside the grains are almost impossible to sustain after solid state sintering [13].

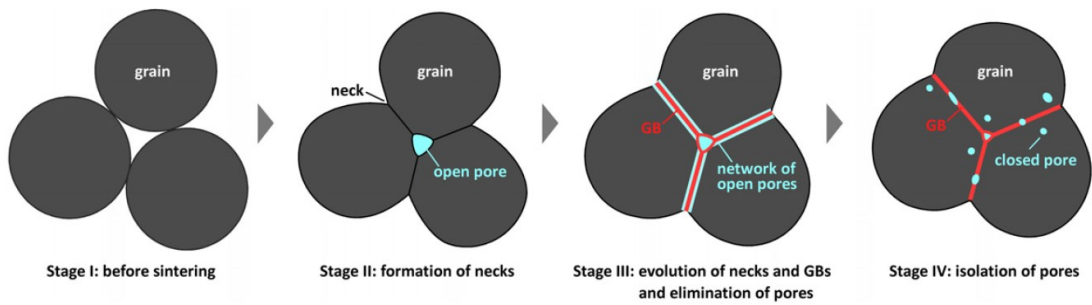


Figure 4. Schematic of solid-state sintering [13]

2.1.4. Liquid Phase Sintering

Existence of the liquid phase of the sintering additives takes a role at the liquid phase sintering. At the sintering temperature of the matrix material, additives change their phase from the solid phase to liquid phase. Liquid phase boosts the bonding rate between the particles with the capillary forces of the liquid on the surface of the particles [14]. As discussed before, solid state sintering cannot eliminate the pores 100%. During the liquid phase sintering, liquid phase of the additives leaks through the pores and eliminates the residual pores and solid grains start to coarsen due to the accelerated diffusion [15].

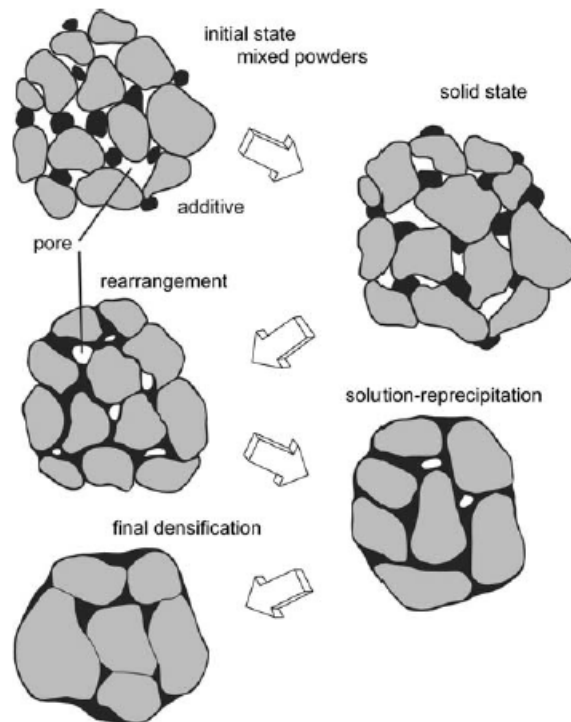


Figure 5. Schematic of the liquid phase sintering [15]

Wetting is another important factor for the liquid phase sintering. An additive with the higher wettability characteristic has to be chosen to activate the liquid phase sintering of the matrix material [15].

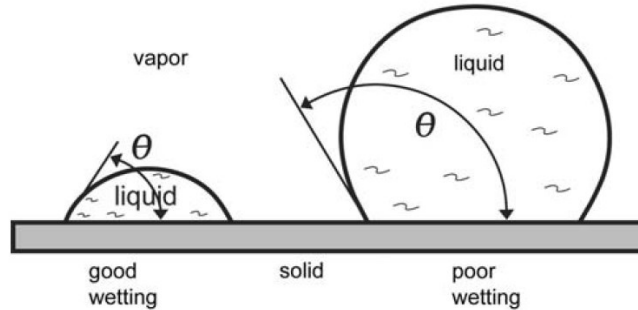


Figure 6. Wetting behavior of the liquid [15]

2.2. Literature Survey about the Effects of Additives on B₄C

Pressureless sintering of the B₄C is a well-studied topic. Due to the oxidation tendency of the boron carbide, inert atmosphere or the vacuum must be provided to sinter and densify the green compacts. While the high sintering temperatures like 2200-2300 °C are necessary to obtain high relative densities, different sintering additives are used to reduce the sintering temperatures at nearly all studies about pressureless sintering of B₄C.

A series of studies show that the pure B₄C is tried to sinter in the range of 2200-2300 °C. 65% relative density is achieved at the 2250 °C by the pioneering study about B₄C which is done by Dole et al [16]. Same study states that 70-72% relative density is obtained at 2300 °C. Lee et al. achieved better results as 92% relative density at 2250 °C [5]. Another study claimed that 78,6% relative density achieved at 2200 °C while 82,5% relative density is obtained at 2250 °C [17].

Owing to the low relative densities, mechanical properties of the final products are lower than the capacity of the B₄C. Sintering additives are the most conventional option to increase the relative densities. While the most common sintering additive is carbon, B, SiC, TiB₂, ZrO₂, Ti, TiO₂, Y₂O₃, Al₂O₃, TiC, BeC, CrB₂, Zr, Cr, Y, La, Al, Si, La₂O₃ are the examples of the used sintering additives in the literature. By means of the sintering additives, secondary phases occur at the microstructure and liquid phase sintering can be activated at the sufficient temperature.

Study of Dole et al. shows that the addition of 6 wt. % C increased the density to 95% at 2300 °C [16]. Lee et al. achieved 98% relative density at 2250 °C with 3 wt. % C addition [5]. Increment of the C amount up to 5% increased the relative density up to 93% at 2250 °C but further increment of the C starts to decrease the relative density at the same parameters [17]. Flexural strength increased with the addition of 3% C from 174 MPa to 350 MPa.

According to the Baharvandi et al., addition of 5-30% TiB₂ increased the relative density from 86% to 98,5% at 2150 °C [18]. Optimum amount of the TiB₂ is 15% for the Vickers hardness and flexural strength values because the higher addition amounts decrease the mechanical properties with one exception. Fracture toughness is the exception because it shows stable increase with the increment of the addition.

Study of Subramanian et al. claims that the 2,5-30% ZrO₂ addition at 2275 °C for 1 hour increased the relative densities from 86,63% to 95,82% [19]. Vickers hardness values are approximately same at all amounts of ZrO₂ as 30-31 GPa. ZrB₂ is observed as a secondary phase at the microstructure.

Another study about ZrO₂ addition is done by the Baharvandi et al. which is increased the relative density from 75% to 98% at the range of 5-30 wt.% ZrO₂ addition at 2150 °C for 1 hour [20]. Highest Vickers hardness value is obtained at the 20% ZrO₂ while the highest fracture toughness and flexural strength are achieved at the 30% ZrO₂.

Levin et al. studied the 5-20% Ti at 2190 °C and 5-20% TiO₂ at 2160 °C as sintering additives and increased the relative densities from 62% to 86% with Ti, from 72% to 95% with TiO₂ [21]. Flexural strength increased continuously from 200 MPa to 420 MPa at the 5-20% TiO₂ addition. Their another study with the coarser B₄C powder at 2190 °C claimed that the relative density is increased from 73% to 93% with the 10-40 wt.% TiO₂ addition [22]. Flexural strength also increased from 120 MPa to 400 MPa.

Lee et al. studied with 1-5 wt.% Al₂O₃ addition and increased the relative density from 85% to 96% at 3% Al₂O₃ at 2150 °C [23]. Higher than 3% addition decreased the relative densities.

Study of Sigl shows the different effect of TiC addition at increased sintering temperature. When the sintering temperature increases from 2150 °C to 2200 °C, fracture toughness and flexural strength decrease [24]. His study claims that the increased TiC amount from 1,5% to 6% decreased the Vickers hardness value even though the relative densities are increased.

Table 1. Effects of the sintering additives on B₄C

Material Composition	Sintering Conditions	Sintered Relative Density	Mechanical Properties	References
B ₄ C + 5 wt. % ZrO ₂	2275 °C, under a dynamic vacuum, 1 hour, pressureless	93 %	Knoop hardness of sintered samples are increased from 24-25 GPa to 32 GPa.	[8]
B ₄ C + 5-30 wt. % ZrO ₂	2275 °C, under a dynamic vacuum, 1 hour, pressureless	93-96 %	Knoop hardness of sintered samples are increased from 27 GPa to 30-31.5 GPa.	[19]
B ₄ C + 3 wt. % C	2250 °C, 0.5L/min He gas flow, pressureless	98.65 %	Reduced the grain size from 2,8 micron to 2,34 micron.	[5]
B ₄ C + 4 wt. % Al	2050-2150 °C, Ar atmosphere, 1 hour, pressureless	94 %	Hardness, fracture strength and elastic modulus increased up to 4 % Al.	[4]
B ₄ C + up to 10 vol. % Al ₂ O ₃	2000 °C, 1 hour, Ar atmosphere, 1 hour, 30 MPa hot press	Almost 100 %	Relative density, hardness and flexural strength increased up to 2.5 vol. % Al ₂ O ₃ .	[9]
B ₄ C + 5 – 30 wt. % Cr ₃ C ₂	2150 °C, under Ar atmosphere, 1 hour, pressureless	95 %	Flexural strength decreases with the increased grain size at high sintering temperatures.	[25]
B ₄ C + 18 wt. % PF + 4 wt. % Dy ₂ O ₃ , Eu ₂ O ₃ , Sm ₂ O ₃	1960-2160 °C, Ar atmosphere, 2 hours, pressureless	91.6-96.6 %	Rare earth oxide additives increased the flexural strength.	[26]
B ₄ C + Metal Oxides	2180 °C, Ar atmosphere, 2 hours, pressureless	97.5-99 %	While the Y ₂ O ₃ addition decrease the strength of the material, TiO ₂ and ZrO ₂ additives maintained the strength of the B ₄ C. Hardness values are lower than the B ₄ C.	[27]
B ₄ C + Al + Si	2226 °C, under vacuum and Ar atmosphere, 4 hours, pressureless	97.4 %	Grain sizes of both B ₄ C and secondary phases are larger at loose compacts.	[28]
B ₄ C + 30 wt. % YTZP	2160 °C, Ar atmosphere, 1 hour, pressureless	97.5 %	Vickers hardness values are varied between 30-33 GPa.	[29]

Table 1 shows the effect of the different sintering additives. Most of the case, mechanical properties and relative densities increase with the optimum amount of sintering additives.

Common effects of the oxide additives like ZrO₂, Al₂O₃, rare earth oxide additives and TiO₂ are increased hardness and increased relative density while the strength of the material is found to be both increased and decreased depending on the additive. The main reason of the increased relative density is liquid phase sintering of the oxide additives with the help of homogeneous dispersion of the additive.

CHAPTER 3

MATERIALS AND EXPERIMENTAL PROCEDURES

Boron carbide was the matrix material of this study due to its advantages. Additives were used in order to reduce sintering temperatures for pressureless sintering. Different methods such as precipitation method, sintering, metallographic procedures and characterization techniques were followed to accomplish this goal.

3.1. Selected Additives and Their Ratio

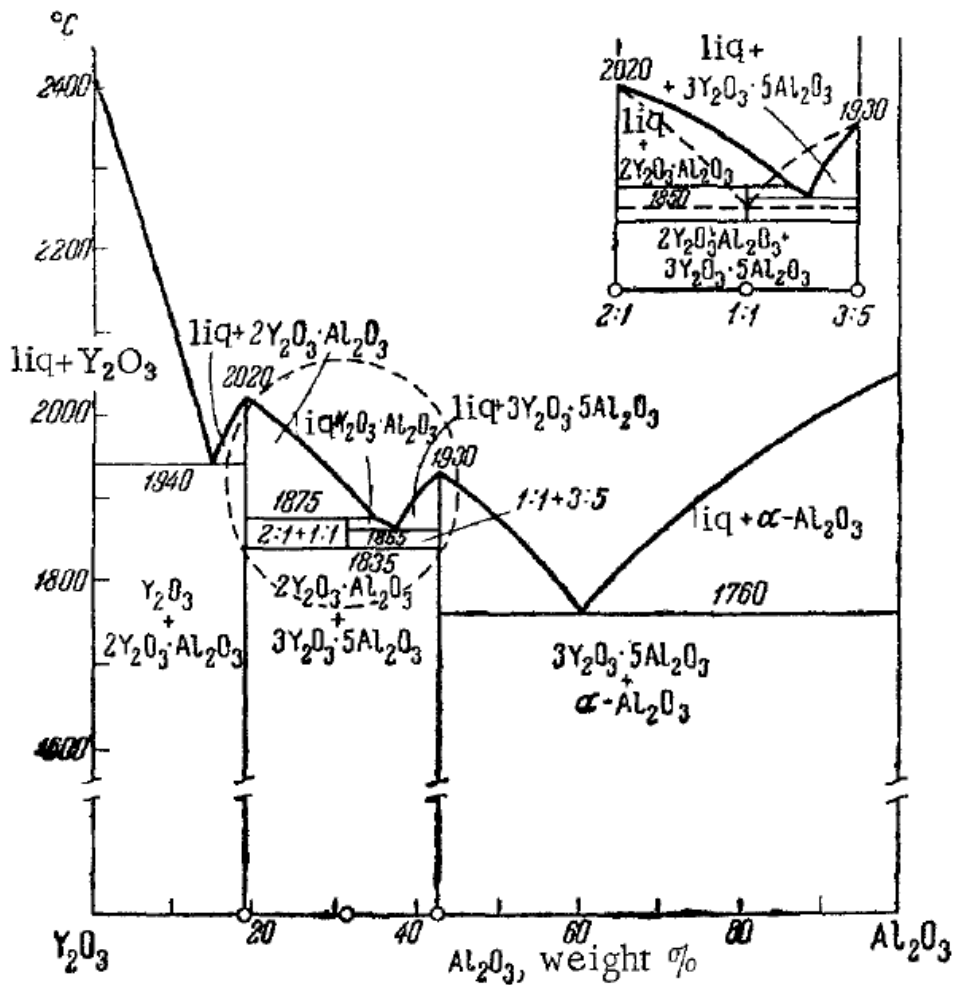


Figure 7. Phase diagram of Al_2O_3 - Y_2O_3 [35]

While the matrix material was chosen as boron carbide, alumina and yttria are the main sintering additives of this study. At some studies, $Y_2O_3 - Al_2O_3$ ratio of 5:2 was chosen to preserve the glassy phase at grain boundaries [30, 31]. In order to deflect the growing crack in a material, brittle intergranular layer was needed and yttrium aluminum garnet (YAG, $Y_3Al_5O_{12}$) was the needed phase for that intergranular layer [32]. Yttrium aluminum monoclinic (YAM, $Y_4Al_2O_9$) and yttrium aluminum perovskite (YAP, $YAlO_3$) are the other phases of the $Al_2O_3 - Y_2O_3$ system [33]. $Al_2O_3 - Y_2O_3$ additives cause a liquid phase with a low viscosity and encourages a rapid diffusion [34]. 60 wt. % $Al_2O_3 - 40$ wt. % Y_2O_3 ratios were selected because of their lowest eutectic point at their phase diagram. Activation of the liquid phase sintering was attained at the $1760^\circ C$ with the help of the lowest eutectic point.

3.2. Precipitation Method as an Improved Processing

Precipitation method was used to distribute the additives as homogeneous as possible. Well distributed additives increase the possibility of activating the liquid phase sintering to reduce the sintering temperature which increases the relative density and improve mechanical properties.

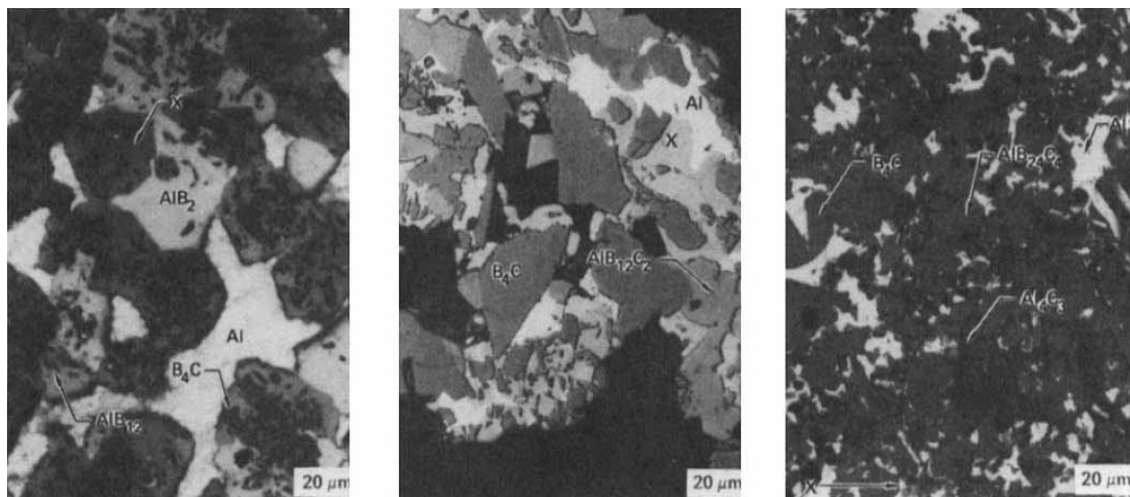


Figure 8. Example of the heterogeneous distribution of the additives and their interphases [37]

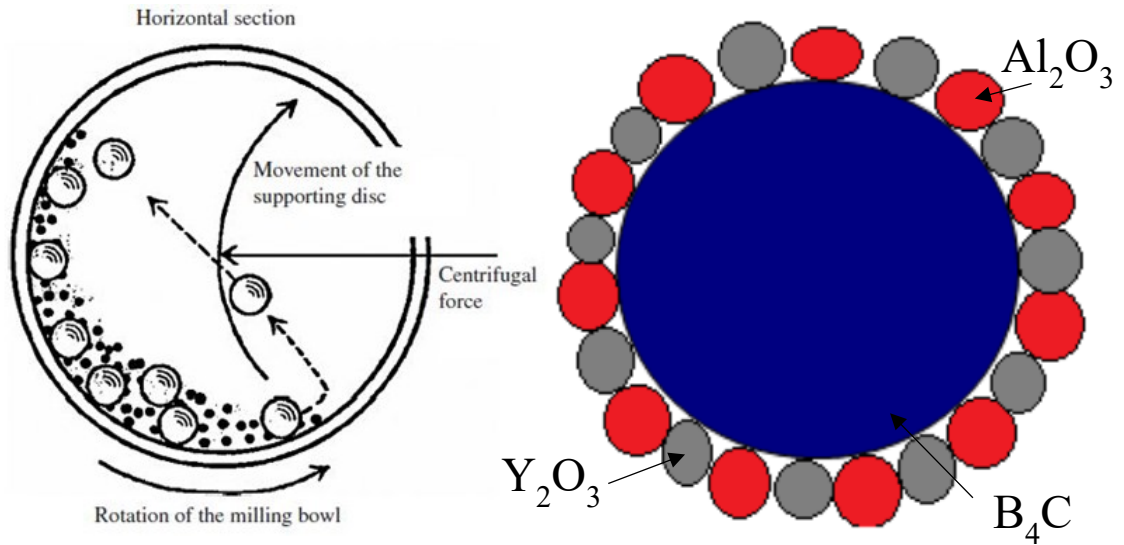


Figure 9. Synthesized powders via the traditional milling method (left) and precipitation method (right)

Insoluble solid additives were nucleated from their metal hydroxides by solving their salt precursors at the solvent. In order to obtain fully homogeneous distribution of the additives, mixture had to be well mixed and supersaturated. Supersaturated mixture could be achieved with the low temperatures, evaporation or increasing pH. Liquid mixing/supersaturation, nucleation, crystal growth and aggregation were the main stages of the precipitation method [36]. During the precipitation process, additives attached to the surface of the suspended material. Another important factor about precipitation method was that it can provide nano sized additive particles.

3.2.1. Procedures of the Precipitation

In order to obtain the most possible homogeneous distribution, all mixtures had to be mixed and stirred for an adequate time. The main requirements for the precipitation of the $Y(NO_3)_3$ and $Al(NO_3)_3$ with the B_4C powders were the well-calculated amounts of the additives, non-ionic surfactant, solvents, pH equalizer, magnetic stirrer and the ultrasonication.

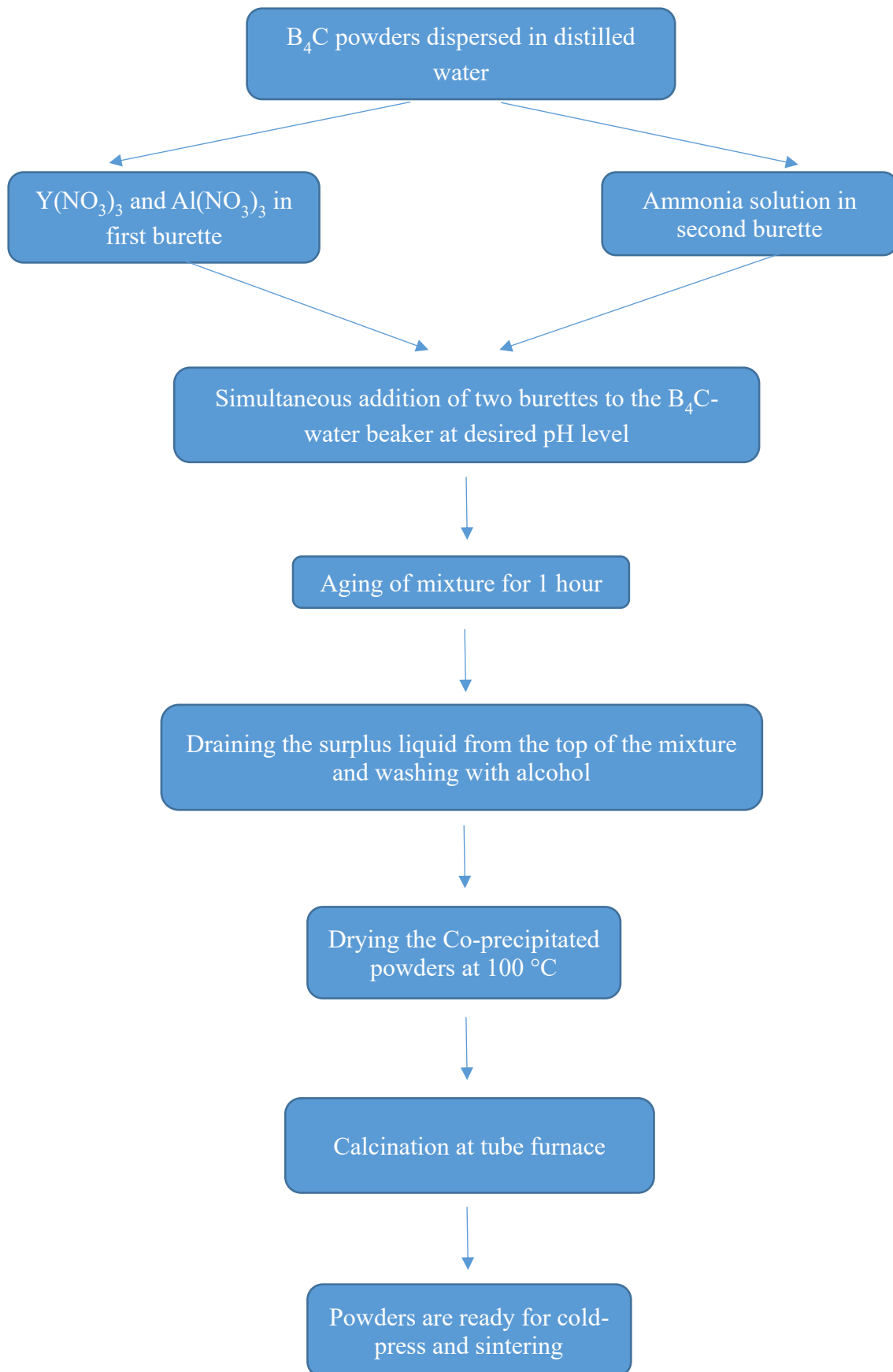


Figure 10. Procedures of the synthesizing of B₄C via the precipitation method

3.2.2. Raw Materials

Boron Carbide: B₄C was chosen because of its high mechanical properties even though it has high sintering temperature. Fine grained powders were selected to sinter at relatively lower temperatures due to the high specific surface area. The properties of the B₄C powder used in this study were shown below;

- B₄C Grade HS (Product of H.C. Starck GmbH)
- Product No: AB134566
- Molecular Weight: 55,26 g/mol
- Density: 2,510 g/ml
- Melting Point: 2450°C
- Boiling Point: 3500°C
- Specific Surface Area: 15-20 m²/g
- Particle Size by Laser Diffraction: 0,6-1,2 μm

Aluminum Nitrate Nonahydrate: Aluminum nitrate was used to obtain the aluminum oxide as a sintering additive. Precipitation process needs nitrate salts to obtain the oxide additives.

- Product of Carlo Erba (Aluminum nitrate nonahydrate RE, 312007)
- Chemical Formula: Al(NO₃)₃.9H₂O
- Molecular Weight: 375,13 g/mole
- CAS No: 7784-27-2

Yttrium Nitrate Hexahydrate: Yttrium nitrate was used to obtain the yttrium oxide as a sintering additive, similar to aluminum nitrate.

- Product of abcr (Yttrium(III) nitrate hexahydrate; (99.9% Y), AB122290)
- Chemical Formula: Y(NO₃)₃.6H₂O
- Molecular Weight: 383,01 g/mole
- Density: 2,682 g/cm³
- CAS No: 13494-98-9

Methanol: Methanol was used for washing the samples to eliminate the oxidation of the powders and the residues of the precipitation process.

- Product of Tekkim (Methanol Extra Pure, TK.120320)

- Chemical Formula: CH₃OH
- Purity: >= 99,8%
- Density: 0,790-0,793 g/cm³
- CAS No: 67-56-1

Isopropanol: Isopropanol (2-Propanol) was used as a solvent of the nitrate salts.

- Product of Carlo Erba (Propan-2-ol RPE - For analysis - ACS - Reag. Ph.Eur. - Reag. USP, 415156)
- Chemical Formula: CH₃CHOHCH₃
- Density: 0,785-0,789 g/cm³
- CAS No: 67-63-0

Ammonia Solution: 25% ammonia solution was used to regulate the pH of the mixture during the precipitation.

- Product of Carlo Erba (Ammonia solution 25% RPE - For analysis, 419993)
- Chemical Formula: NH₄OH
- Density at 20° C: 0,901-0,907 g/cm³
- CAS No: 1336-21-6

Triton X-100: Triton which is a nonionic surfactant was used to increase the suspension time of the precipitation process.

- Product of Merk (Triton X-100 for analysis, 1.08603.1000)
- Chemical Formula: C₈H₁₇C₆H₄(OCH₂CH₂)_nOH
- Density at 20° C: 1,064-1,067 g/cm³
- pH: 6-8
- Cloud Point: 63-69° C
- CAS No: 9036-19-5

Distilled Water: Distilled water was also used as a solvent like isopropanol and supplied from the laboratory water distiller of İYTE.

3.2.3. Initial pH Studies

Precipitation process needed stable pH value to keep the surface characteristics of the B₄C powders balanced. Solubility of the nitrate salts was an important factor for the

precipitation of the oxides and pH increase eases the precipitation with the help of supersaturation [36]. pH value of the precipitation was determined by drawing the titration curves of the B₄C and nitrate salts and finding the equivalence point of all of them.

HCl and KOH were used to regulate the pH of the solutions.

- 2 different 200 ml 0,01 vol.% B₄C-H₂O solution were prepared with the help of magnetic stirrer at 200 rpm. (0,05 g B₄C – 200 ml distilled water)
- 0,1 M HCl was prepared. (0,828 ml HCl- 100 ml distilled water)
- 0,1 M KOH was prepared. (0,561 gr KOH pellets – 100 ml distilled water)
- HCl was dropped to first beaker to decrease the pH (increase the acidity) of the solution while the magnetic stirrer is continuously working.
- KOH was dropped to second beaker to increase the pH (increase the basicity) of the solution while the magnetic stirrer is continuously working.
- pH meter was continuously measured the pH value of the solution.

3.2.4. Calculations of the Precipitation Method

Molar Weights of the Nitrate Salts:

$$Y(NO_3)_3 \cdot 6H_2O = 383,01 \text{ g/mole}$$

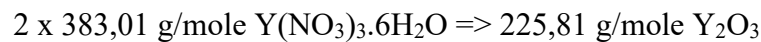
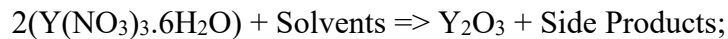
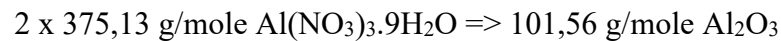
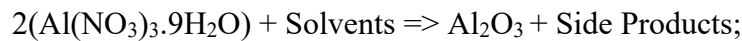
$$Al(NO_3)_3 \cdot 9H_2O = 375,13 \text{ g/mole}$$

Molar Weights of the Expected Additives:

$$Al_2O_3 = 101,96 \text{ g/mole}$$

$$Y_2O_3 = 225,81 \text{ g/mole}$$

Chemical Formula of the Reactions:



Necessary Aluminum Nitrate Amount to Obtain Alumina:

10 g B₄C - Al₂O₃ Mixture with 3 wt. % Al₂O₃;

2,208 g - 0,006 mole Al(NO₃)₃·9H₂O is necessary to obtain 0,3 g Al₂O₃

10 g B₄C - Al₂O₃ Mixture with 6 wt. % Al₂O₃;

4,416 g - 0,012 mole Al(NO₃)₃·9H₂O is necessary to obtain 0,6 g Al₂O₃

Necessary Yttrium Nitrate Amount to Obtain Yttria:

10 g B₄C - Y₂O₃ Mixture with 2 wt. % Y₂O₃;

0,68 g - 0,00176 mol Y(NO₃)₃.6H₂O is necessary to obtain 0,2 g Y₂O₃

10 g B₄C - Y₂O₃ Mixture with 4 wt. % Y₂O₃;

1,356 g - 0,00352 mol Y(NO₃)₃.6H₂O is necessary to obtain 0,4 g Y₂O₃

3.3. Characterization Techniques

Zeta potential, XRD, cutting, grinding, polishing of the specimen, SEM analysis and porosity analysis via ImageJ software were the main characterization techniques of this study.

3.3.1. Zeta Potential

The principle of zeta potential method was to analyze the surface charge of the particle. Zeta potential values of the pure B₄C and the precipitated powders were compared to observe the success of the process. Isoelectric point was the point where the surface charge of the particle equals to 0. Additives and oxide layers changed the isoelectric point of the pure powders due to the coating characteristic. Isoelectric points of the powders were compared to understand the success of the process.



Figure 11. Zetasizer Nano device [38]

HCl and KOH were used to regulate the pH of the solutions.

- 2 different 200 ml 0,01 vol.% B₄C-H₂O solution were prepared with the help of magnetic stirrer at 200 rpm. (0,05 g B₄C – 200 ml distilled water)
- 0,1 M HCl was prepared. (0,828 ml HCl- 100 ml distilled water)
- 0,1 M KOH was prepared. (0,561 gr KOH pellets – 100 ml distilled water)
- HCl was dropped to first beaker to decrease the pH (increase the acidity) of the solution while the magnetic stirrer is continuously working.
- KOH was dropped to second beaker to increase the pH (increase the basicity) of the solution while the magnetic stirrer is continuously working.
- 10 milliliters of solutions with different pH values as 4-5-6-7-8-9 pHs were collected for zeta potential analysis.
- Zetasizer Nano Series Disposable Folded Capillary Cell (DTS 1070) was used to drop the prepared solutions into it. Cell was placed inside the device for analysis.
- Analysis was done with Zetasizer Nano device at the Chemical Lab of the İYTE. (All standard parameters were used except the test cycle number. Cycle number was increased from 3 to 6.)
- Zetasizer software was used to investigate the results and Origin software was used to draw a graph from collected data.

3.3.2. X-Ray Diffractometry



Figure 12. X-Ray Diffraction device [39]

X-Ray diffraction (XRD) method used the crystal structure of the elements and compounds by diffracting the x-ray beams. All crystals had different XRD patterns and XRD method used these patterns to identify the unknown powders. Count numbers of the peaks showed the intensity of the elements and compounds in the powder. Pure and precipitated powders were analyzed to examine the oxidation. All analyses were done along 1 hour between 10-80° (2 theta). Obtained data was examined by X'Pert Highscore Plus software. Philips X'Pert Pro device was used for all XRD analyses at the İYTE MAM.

3.3.3. Sintering, Cutting, Grinding, Polishing

Processed and commercial powders were pressed to form pellets. 12 mm diameter mold was used for cold press. 1 gr of powder was pressed with 22700 kg (50000 pounds) force equals to 2 GPa pellet pressure. Prepared samples were put into the alumina crucible in order and crucible was placed inside an alumina tube. Tube was placed in front of the gas outlet of the high temperature furnace to sustain the inert atmosphere. Ramping stages of the furnace were room temperature to 1500 °C with 10 °C/min increment and 1500 °C to 1750 °C with 5°C/min increment. Dwell time was 3 hours at 1750 °C and cooling cycle was ramped to -10 °C/min to room temperature. Valve of the Argon gas was opened at 100 °C manually with 2 l/min flow rate to keep the atmosphere inert.



Figure 13. High temperature furnace

Sintered samples were cut with Struers Minitom tabletop precision cutting device. Diamond cut-off disc was used with varying speeds as 100-200 rpm.

Cut samples were mounted with Struers CitoPress-5 hot press equipment. Standard parameters were used and samples were mounted at 180° C with black phenolic powder as Metkon BAK-B 29-001 Hot Mounting Resin.



Figure 14. Grinder-Polisher device

Metkon Forcipol 2V Grinder-Polisher with Dosione and Forcimat specimen mover were used for the grinding and polishing purpose. All functions of the device were used to standardize and automate the process.

Metkon DEMPAX 38-040-S SiC paper grinding discs were used for grinding. 600 and 1000 grit papers were used for grinding.

Grinding Parameters for 600 and 1000 Grit Papers:

- Tap water as lubricant and heat distributor
- 10 N specimen load
- Forward motion and 150 rpm paper speed
- Clockwise motion and 75 rpm specimen mover speed
- 3 minutes grinding duration for both papers

Metkon METAPO-P 39-013-250 Fine Woven Cloth, DIAPAT-M 6m 39-430-M Water Based 6 micron Diamond Solution, DIAPAT 39-502 Water Based Diamond Lubricant, FEDO-1S 39-066-250 Flock Polishing Cloth, DIAPAT-M 1m 39-410-M Water Based 1 micron Diamond Solution, COLLO 39-085-250 Chemo-mechanical Cloth, COL-K 39-600 Colloidal Silica were used for polishing.

Polishing Parameters for 1st Step:

- DIAPAT 39-502 Water Based Diamond Lubricant was automatically feeded from Dosione
- Forward motion and 100 rpm METAPO-P 39-013-250 Fine Woven Cloth speed
- DIAPAT-M 6m 39-430-M Water Based 6-micron Diamond Solution was sprayed twice onto the cloth
- Counter-clockwise motion and 50 rpm specimen mover speed
- 15 N specimen load
- 5 minutes polishing duration

Polishing Parameters for 2nd Step:

- DIAPAT 39-502 Water Based Diamond Lubricant was automatically feeded from Dosione
- Forward motion and 100 rpm FEDO-1S 39-066-250 Flock Polishing Cloth speed
- DIAPAT-M 1m 39-410-M Water Based 1 micron Diamond Solution was sprayed twice onto the cloth.
- Counter-clockwise motion and 50 rpm specimen mover speed
- 15 N specimen load
- 5 minutes polishing duration

Polishing Parameters for 3rd Step:

- Forward motion and 50 rpm COLLO 39-085-250 Chemo-mechanical Cloth speed
- COL-K 39-600 Colloidal Silica was poured until the liquid spread onto the cloth homogenously
- Counter-clockwise motion and 50 rpm specimen mover speed
- 10 N specimen load
- 2 minutes polishing duration

3.3.4. Scanning Electron Microscopy

After the polishing process, samples were taped with aluminum and coated with gold to increase the reflectivity of the electron beams coming from the Scanning Electron Microscopy (SEM). All samples were carefully investigated at high magnifications with both secondary electron mode and back-scatter electron mode.



Figure 15. SEM device [39]

Secondary electron mode aimed to analyze the topography of the sample to correctly obtain the 3D surface information as shapes or pores. Back-scatter electron mode collected the diffraction data of the sample to differentiate each element by showing different brightness at different areas. Elements with high molecular weight had high brightness than the others in the image.

EDS maps were also obtained with back-scatter electron mode to show the distribution of the elements. All analyses were done by FEI QUANTA 250 FEG microscope at the İYTE MAM.

3.3.5. Porosity Analysis via ImageJ Software

Porosity analysis was done with open source ImageJ image processing software. Even if the Archimedes method was widely accepted way of measuring the density and porosity of the sintered samples, ImageJ software was used to measure the porosity because the sintered samples had lots of cracks and could not hold themselves together under water. Threshold of the SEM images of the samples was adjusted until the pores are painted in black to form an opinion about the porosity.

CHAPTER 4

RESULTS AND DISCUSSION

4.1. Initial Studies

In order to successfully precipitate the additives of boron carbide, stable pH value of precipitation process has to be found. Equivalence point of all of the additives and commercial boron carbide was determined to find a common point.

While the equivalence points of B₄C and aluminum nitrate are close to each other, aluminum nitrate is higher than all of them. As seen in Figure 16, 9,5 pH value is chosen in order to successfully precipitate the additives although the equivalence point of yttrium nitrate is 8 pH.

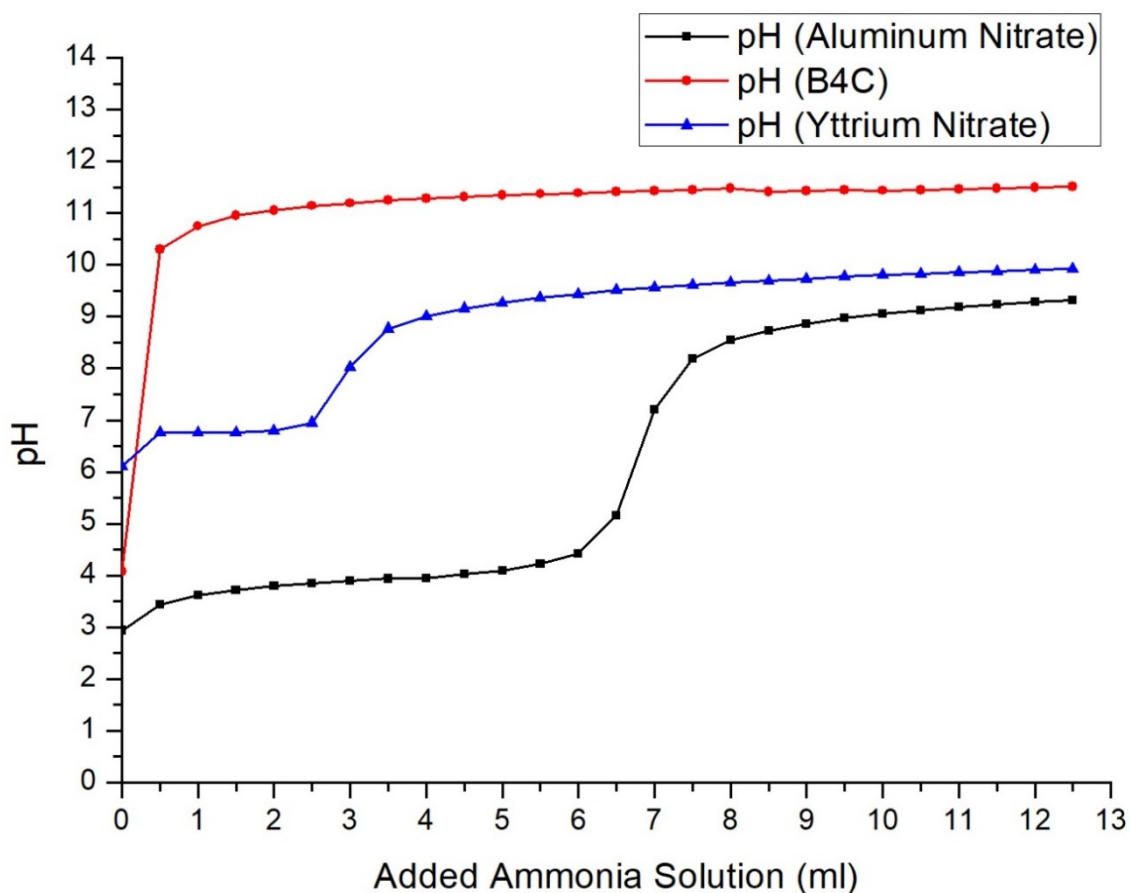


Figure 16. Titration curves of the raw materials

X-Ray Diffraction analysis is done to the raw B₄C powder to investigate the purity of the powders and the result can be seen in Figure 17. C peak is observed as expected because of the residual C left from the production of the B₄C. Other unusual peak belongs to the B₂O₃ due to the oxidation of the powder. That oxide peak has a low intensity and can be easily eliminated with the methanol washing.

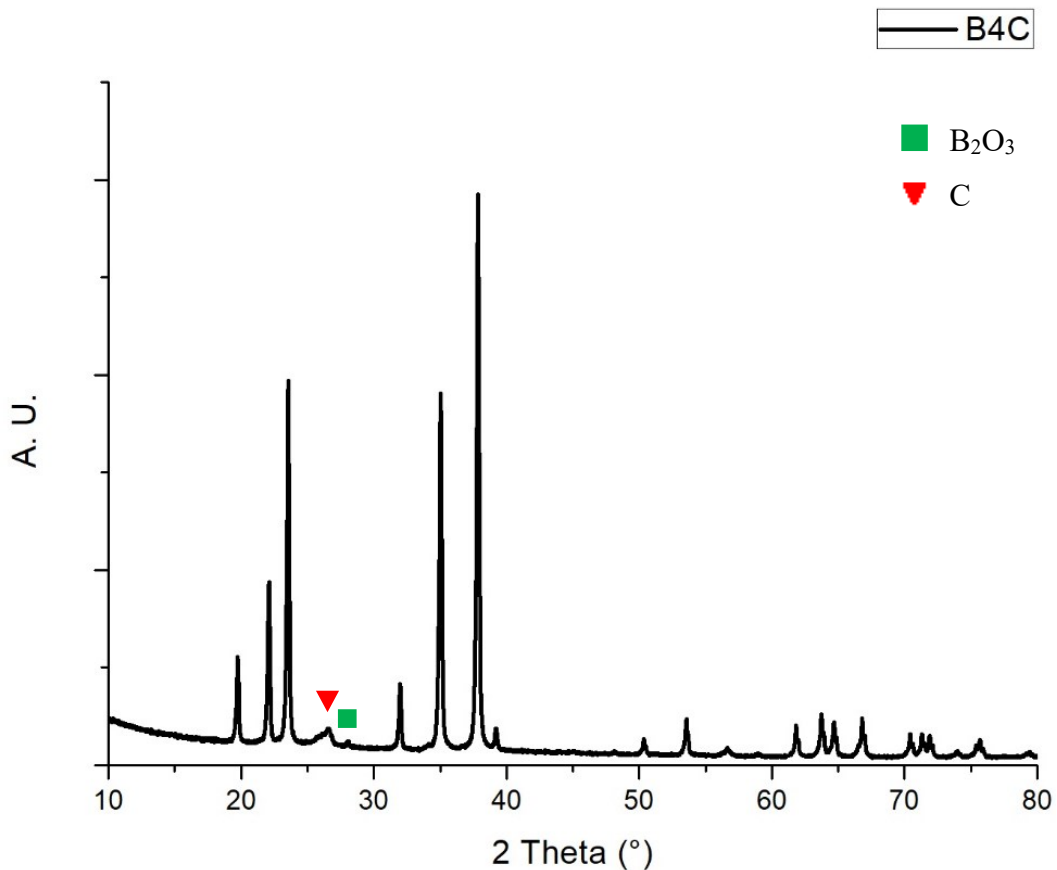


Figure 17. XRD graph of the unprocessed B₄C

Zeta potential analysis is done to find the isoelectric point of the B₄C. As shown in Figure 18, unprocessed powders have a isoelectric point as 5,2 pH while the methanol washed powders have a lower value of isoelectric point as 4.7 pH. Eliminating the oxide layer above the surface of the B₄C with methanol washing reduces the isoelectric point and ensures that the correct isoelectric point of pure B₄C can be measured.

Sharp and micron sized B₄C particles are observed at high magnifications with the secondary electron mode of the SEM (see Figure 19). Secondary electron mode (ETD) is used to clearly investigate the surface and morphology of the powders.

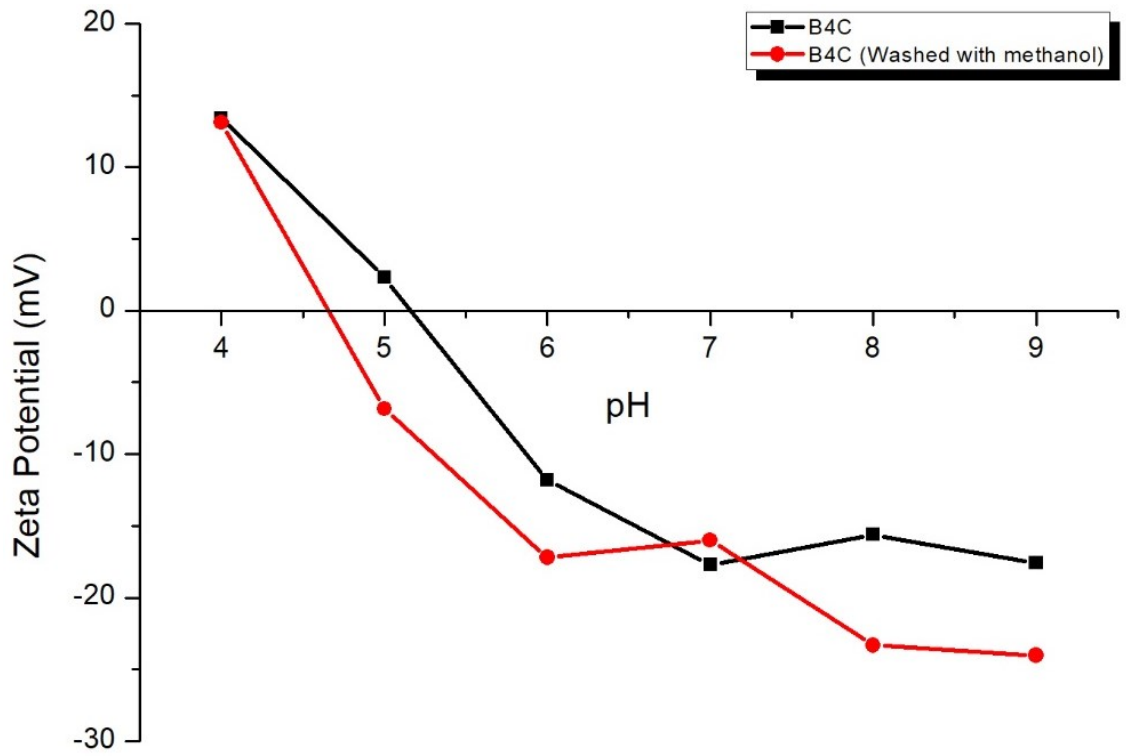


Figure 18. Zeta Potential graph of the B₄C

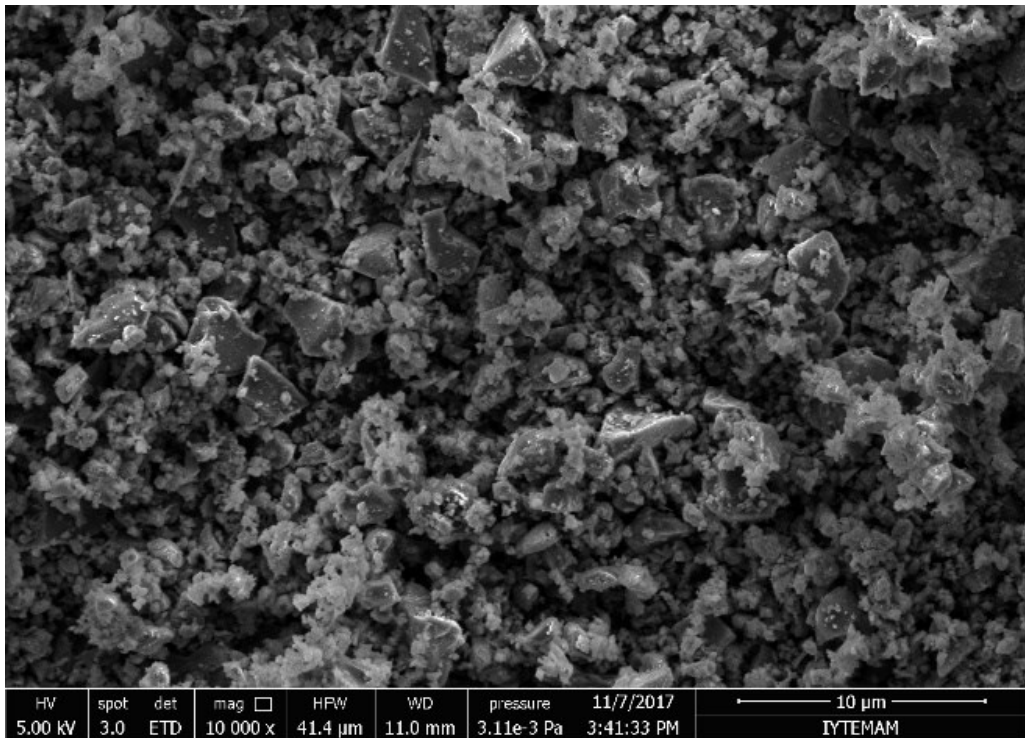


Figure 19. SEM image of the commercial boron carbide particles at high magnification

4.2. Precipitation Studies of Boron Carbide

4.2.1. Powder Analysis of Precipitated B₄C Powders with the Oxide Additives Calcined under Ambient Atmosphere

First of all, precipitation studies are performed under ambient atmosphere to precipitate the additives on boron carbide particles. Al₂O₃ and Y₂O₃ are the additives and first study conducted to obtain 3% Al₂O₃ and 2% Y₂O₃. Nitrate salts of the additives and ammonia solution are simultaneously added to the boron carbide-distilled water beaker while the pH is kept stable at 9,5. After the precipitation, powders are calcined at the tube furnace to eliminate the residual inorganics at 400 °C.

All the peaks of B₄C were observed in Figure 20 with the high intensity B₂O₃ peaks. These oxide peaks are the results of the calcination process at 400°C under the atmosphere of air. Peaks of Al₂O₃ and Y₂O₃ cannot be observed at first glance because of the low amounts of additives.

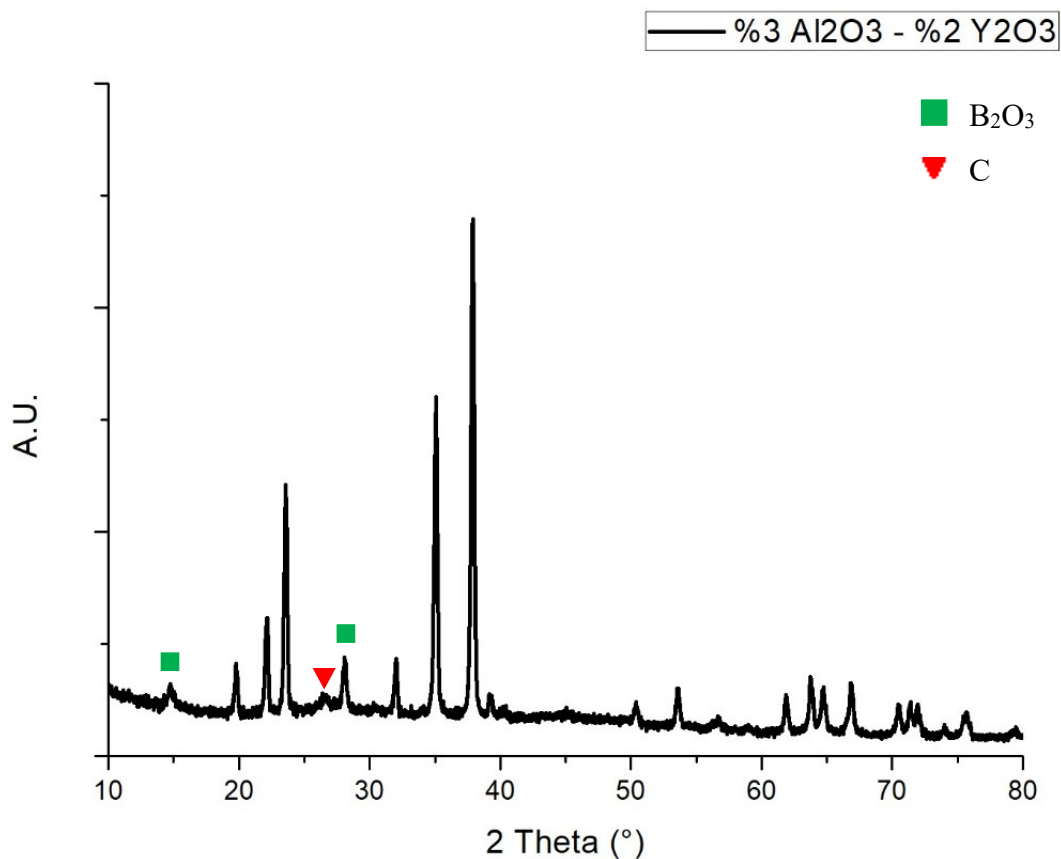


Figure 20. XRD graph of the precipitated B₄C powders with the additives of 3% Al₂O₃ + 2% Y₂O₃

Isoelectric point of the synthesized particles is moved further to the right side of the axis as expected (see Figure 21). The reason behind this change is the attached additive particles above the surface change the surface charge of the B₄C and isoelectric point of synthesized powders become closer to the isoelectric point of the additives. This change shows the success of the precipitation method.

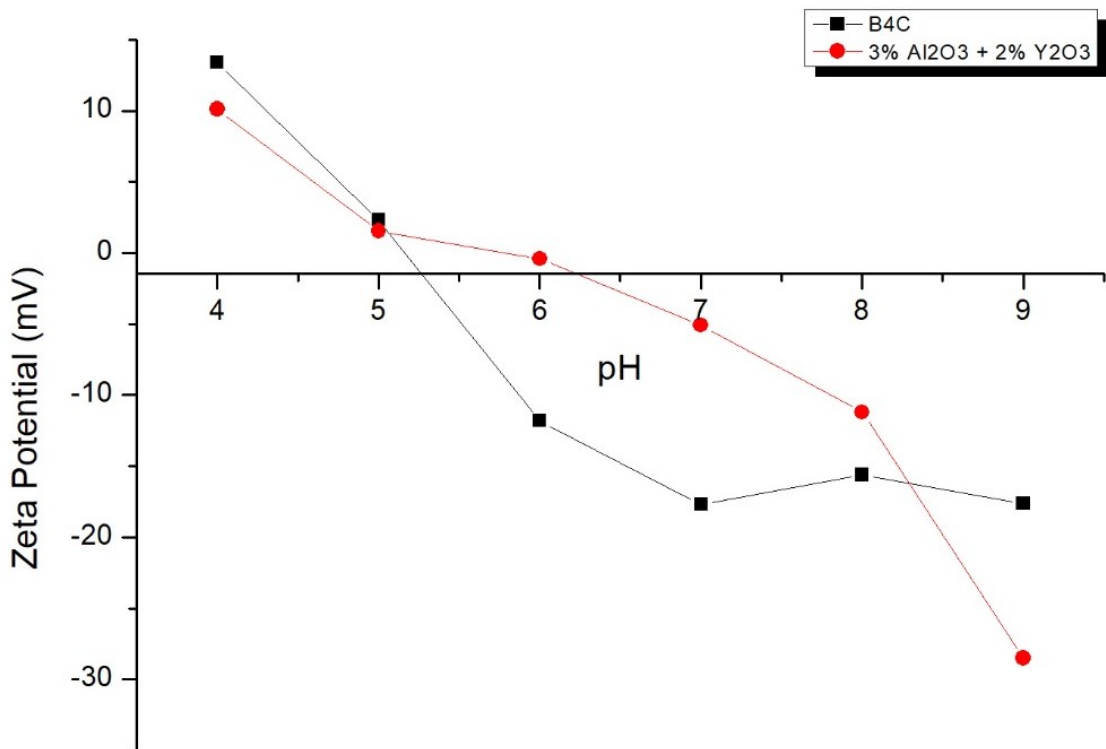


Figure 21. Zeta potential graph of the precipitated B₄C powders with the additives of 3% Al₂O₃ + 2% Y₂O₃

Due to the drying process, analyzed powders are agglomerated even the crushing process is done. B₄C powders are significantly apparent in Figure 22 and 23 other than the precipitated additives. Additives can be seen with the secondary electron mode at the surface of the B₄C powders at the high magnification. Bright areas at the images of the back-scatter electron mode show that the surface of the B₄C is coated with the additives successfully.

After the first study, amount of the additives is doubled to analyze the precipitated powders. Especially the surface characteristic is investigated because of the increment of additive amount. In theory, when the amount of the additive increases, coating will be thicker and uncoated areas will be disappeared.

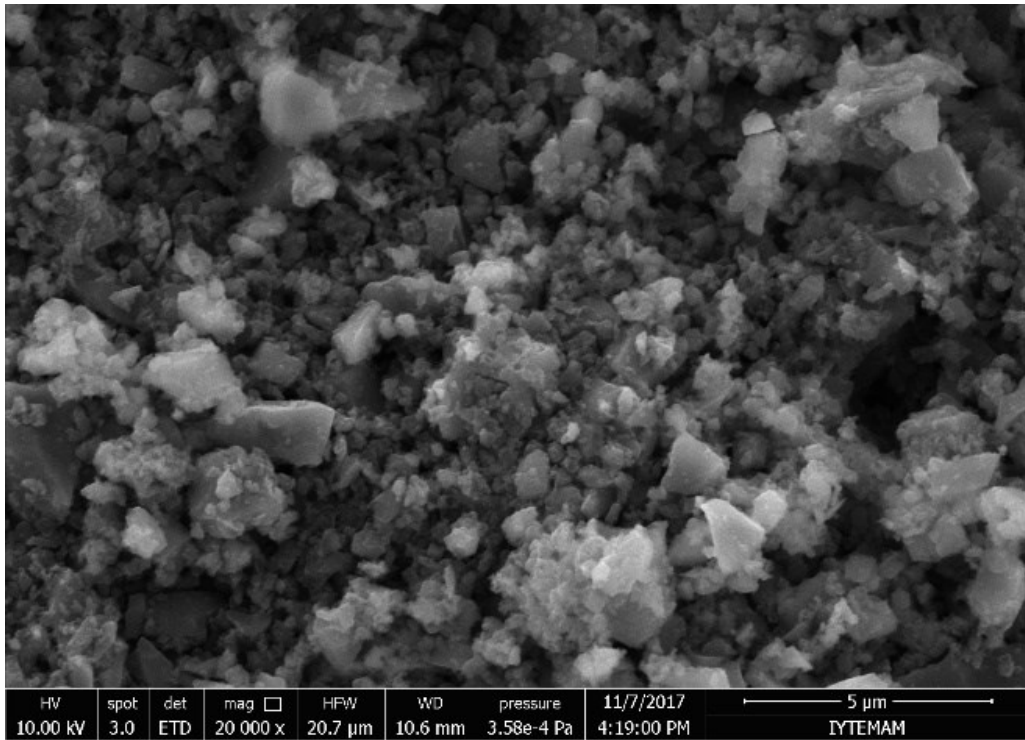


Figure 22. SEM (secondary electron mode) image of the precipitated B₄C powders with the additives of 3% Al₂O₃ + 2% Y₂O₃ at high magnification

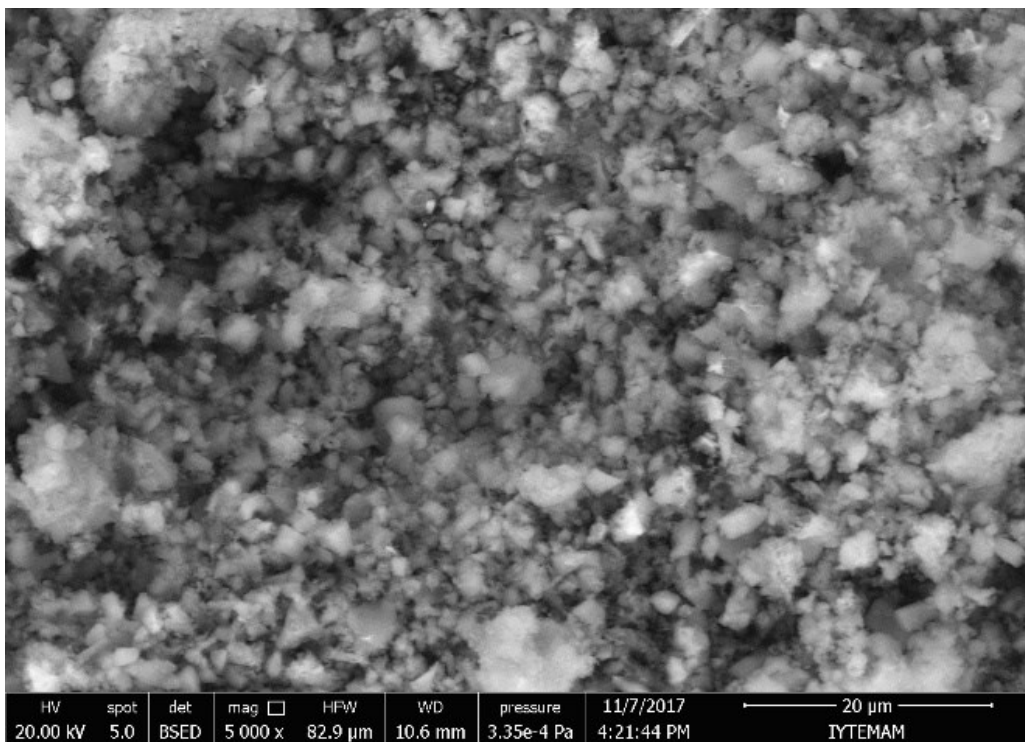


Figure 23. SEM (backscatter electron mode) image of the precipitated B₄C powders with the additives of 3% Al₂O₃ + 2% Y₂O₃ at low magnification

Peaks of the synthesized powders at the XRD graph seems like almost same as the powders with additives of 3% Al_2O_3 + 2% Y_2O_3 . Double amounts of additives do not change the peak pattern as well as the C and B_2O_3 peaks which can be seen in Figure 24.

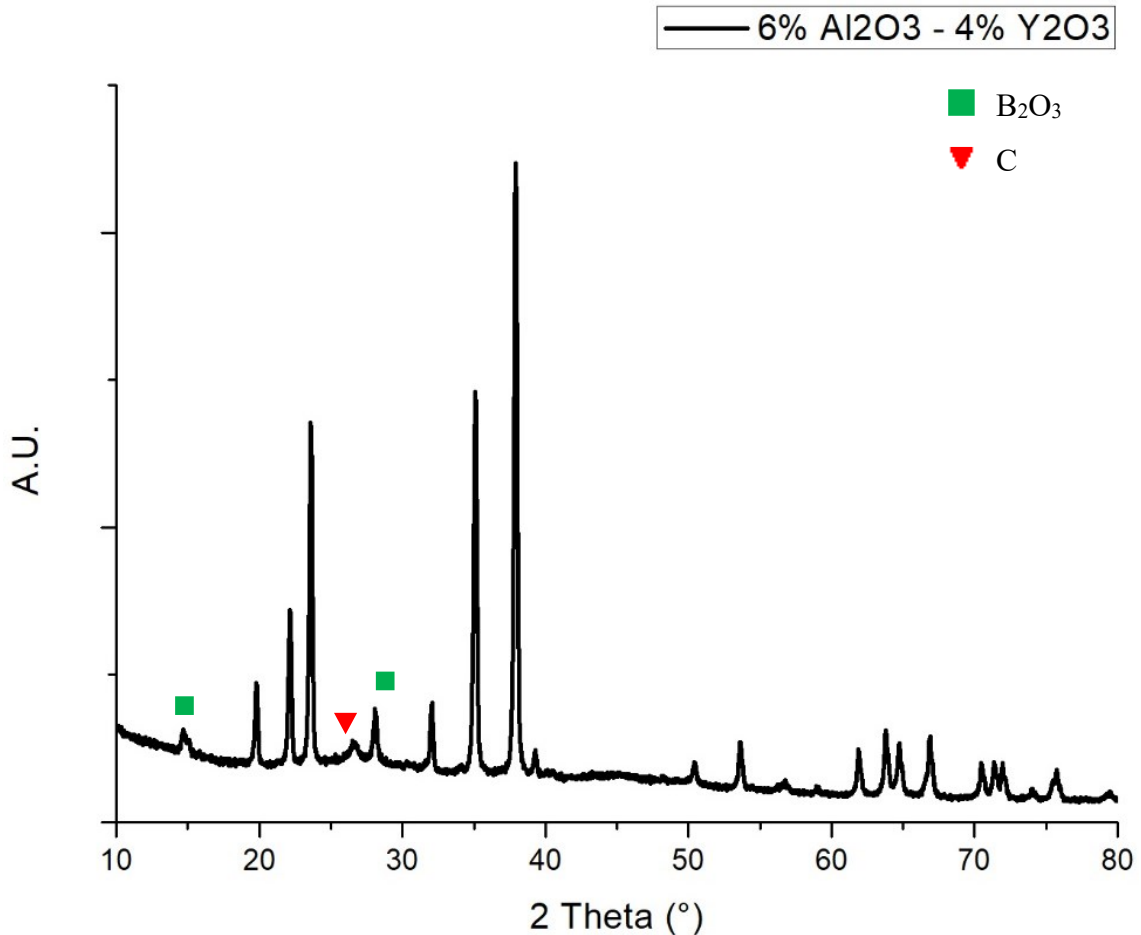


Figure 24. XRD graph of the precipitated B_4C powders with the additives of 6% Al_2O_3 + 4% Y_2O_3

While the graph of the synthesized powders looks similar to the powders with 3% Al_2O_3 + 2% Y_2O_3 additives, isoelectric point of the synthesized powders falls below the B_4C . The probable reason of this situation is the oxide layer above the surface of the synthesized powders (see Figure 25). The reason behind that oxide layer comes from the calcination process. Calcination at ambient atmosphere increases the oxidation rate of the boron carbide powders. Because of that, graph of the precipitated powders is similar to the graph of the commercial boron carbide powders.

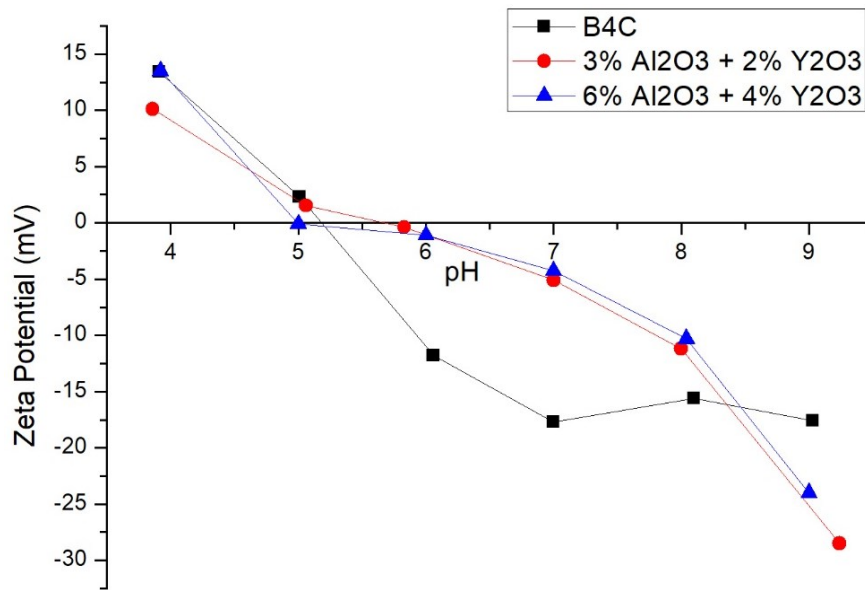


Figure 25. Zeta potential graph of the precipitated B₄C powders with the additives of 6% Al₂O₃ + 4% Y₂O₃

As seen in Figure 26 and 27, SEM images with high magnification show that the additives are successfully attached to the surface of the B₄C powders while the back scatter electron mode shows some areas bright. These bright areas show the existence of higher atomic number elements such as yttrium and aluminum.

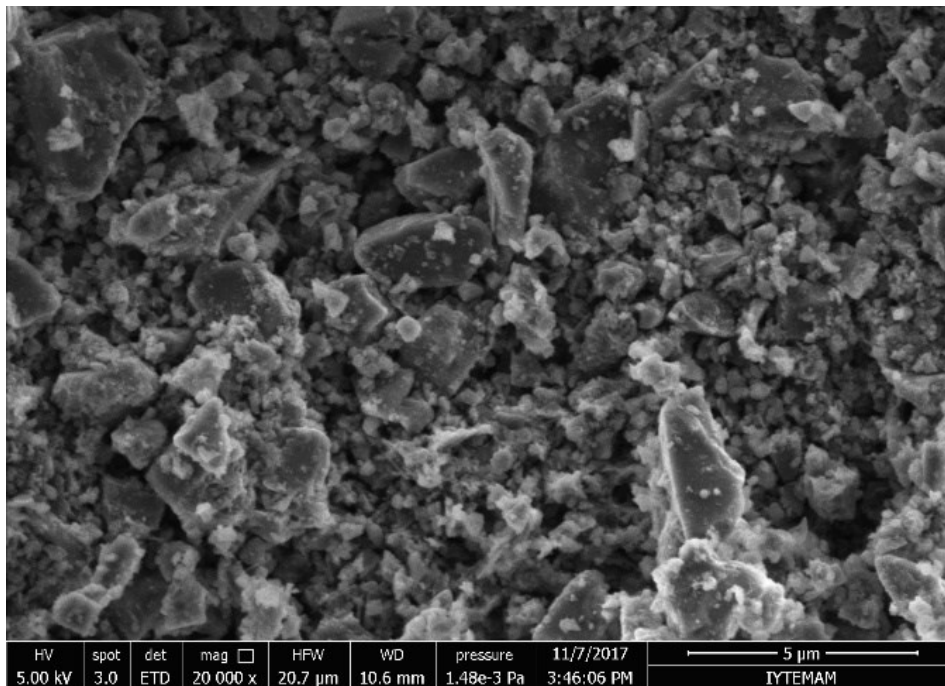


Figure 26. SEM (secondary electron mode) image of the precipitated B₄C powders with the additives of 6% Al₂O₃ + 4% Y₂O₃ at high magnification

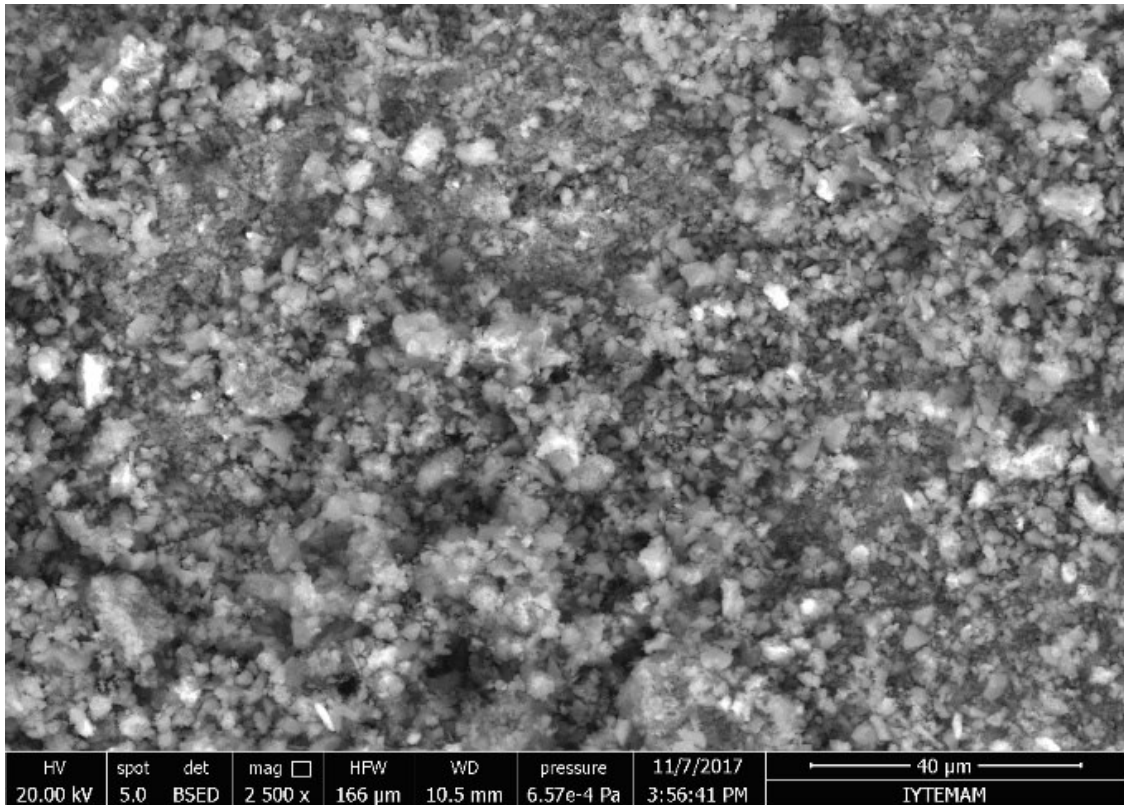


Figure 27. SEM (backscatter electron mode) image of the precipitated B₄C powders with the additives of 6% Al₂O₃ + 4% Y₂O₃ at low magnification

Oxidation and dispersion are the main problems at this point. According to the B₂O₃ peaks at the XRD graph and low isoelectric point value at the zeta potential graph, oxidation problem has to be eliminated at the next studies. SEM images also show the elements with high atomic numbers and they are not dispersed homogeneously throughout the images.

4.2.2. Powder Analysis of Precipitated B₄C Powders with the Oxide Additives Synthesized with 2 Burettes Calcined under Ambient Atmosphere

After the study with double amount of oxide additives, precipitation process improved with 2 burettes. While the nitrate salt of the Al₂O₃ poured into the beaker with one burette, nitrate salt of the Y₂O₃ poured with separate burette. Ammonia solution is added to the mixture with syringe to keep the pH value at 9,5. The reason behind that trial is improving the dispersion of the additives by adding them to the mixture separately.

XRD analysis shows that the pattern of the sample is same as the powders precipitated with conventional method. But the main difference is the oxide peaks have a low intensity at the powders precipitated with 2 burettes (see Figure 28). The probable reason behind the oxide peaks is the calcination atmosphere which includes oxygen. Oxygen reacts with the boron at high temperatures as 400 °C and forms boron oxide as a result.

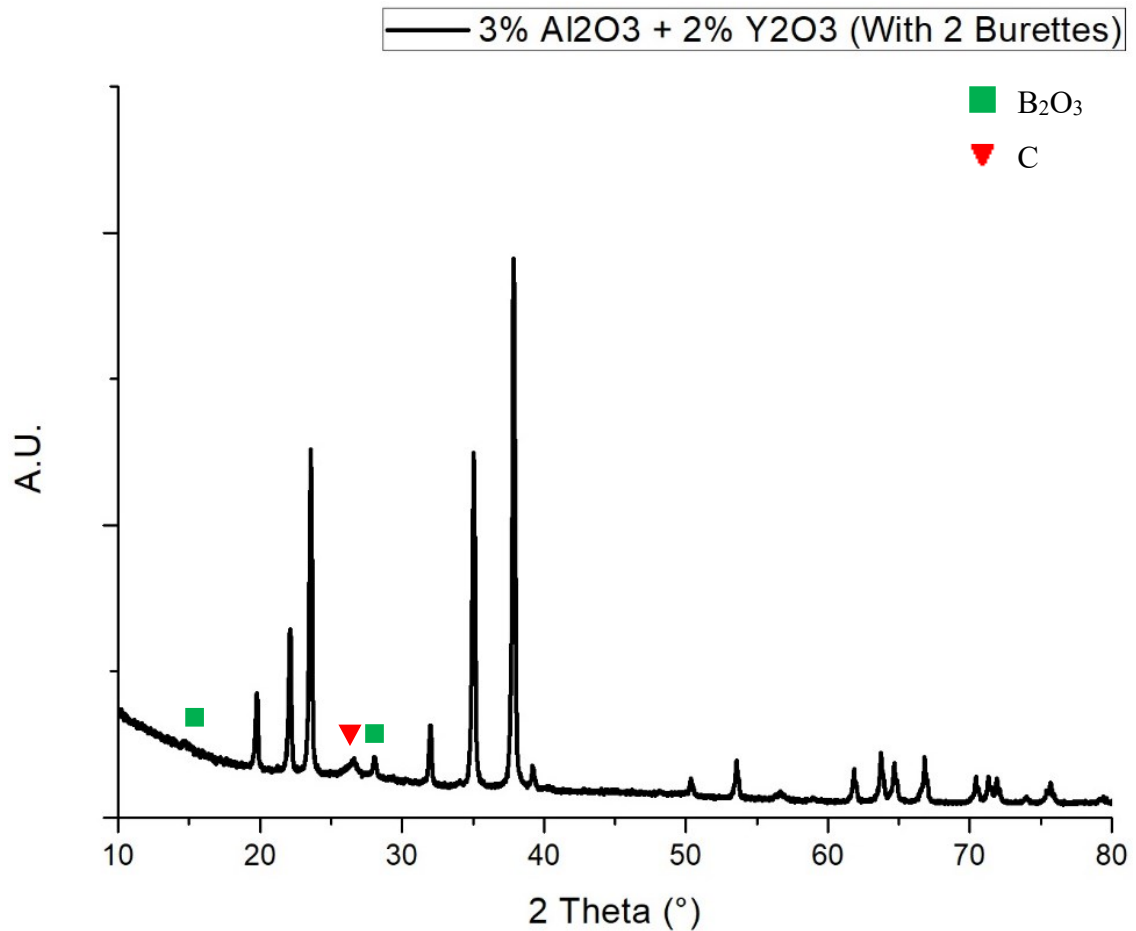


Figure 28. XRD graph of the precipitated B₄C powders with the additives of 3% Al₂O₃ + 2% Y₂O₃ (Precipitated with 2 burettes)

Zeta potential analysis shows that the isoelectric point of the synthesized powders has a same value as the powders precipitated with conventional method. As shown in Figure 29, isoelectric point moves further to 8,2 pH as desired after washing with methanol to eliminate the oxide layer. Fluctuation of the graph may be the reason of irregular additive coating on the surface of the boron carbide particles. That fluctuation

can be related with additive amount, stirring duration of mixture or suspension time during the precipitation process.

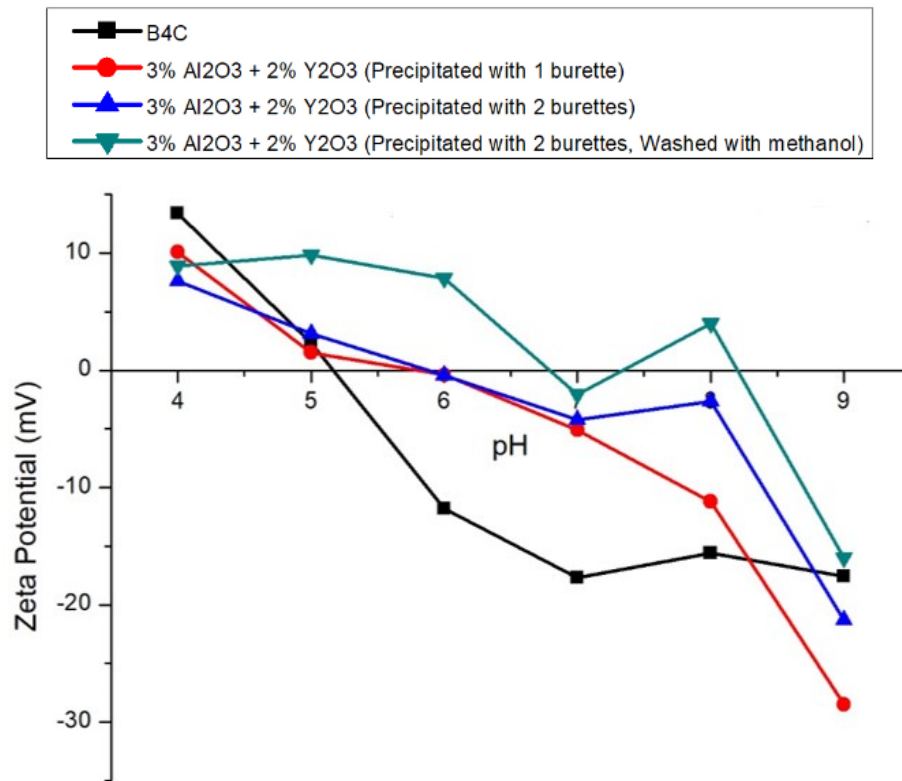


Figure 29. Zeta potential graph of the precipitated B₄C powders with the additives of 3% Al₂O₃ + 2% Y₂O₃ (Precipitated with 2 burettes)

As a result of this study, oxidation is still a problem and dispersion is not homogeneous enough to obtain smooth curve at zeta potential graph. Precipitated and unwashed powder has an almost same isoelectric point with the sample precipitated with 1 burette. Methanol washing eliminates the oxide layer but washed sample has a fluctuation at the zeta potential curve.

4.2.3. Powder Analysis of Precipitated B₄C Powders with the Oxide Additives Calcined under Ar Atmosphere

In order to eliminate the observed B₂O₃ peaks of previous studies, calcination atmosphere was changed to Argon atmosphere from ambient atmosphere. Because Argon

is an inert gas, boron carbide particles cannot react with oxygen to form B_2O_3 at high temperatures.

XRD patterns show that calcination under Ar atmosphere prevents the formation of the oxide layer. Figure 30 shows that the pattern of synthesized powders is similar to the powders precipitated with conventional method except the B_2O_3 peaks.

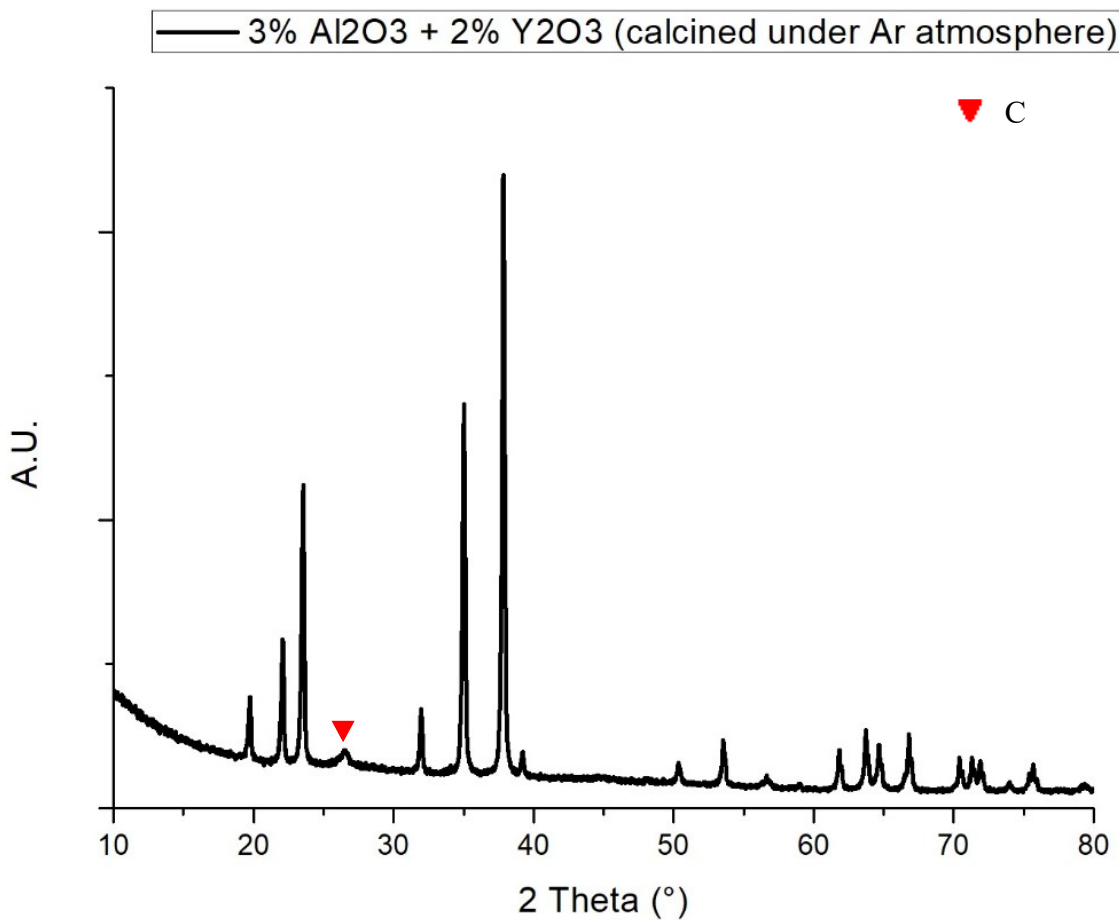


Figure 30. XRD graph of the precipitated B_4C powders with the additives of 3% Al_2O_3 + 2% Y_2O_3 (Calcined under Ar atmosphere)

As seen in Figure 31, isoelectric point of the sample is measured as 6 pH as same as powders synthesized with conventional precipitation method. But, trend of the graph is generally higher than the conventional method. Even if the XRD analysis cannot observe the oxide peaks, low level of isoelectric point states the proof of the oxide layer. Isoelectric point increases to 8,3 pH after the methanol washing of the powders. Methanol washing eliminates the B_2O_3 layer and yttria and alumina coated boron carbide surfaces increases the isoelectric point.

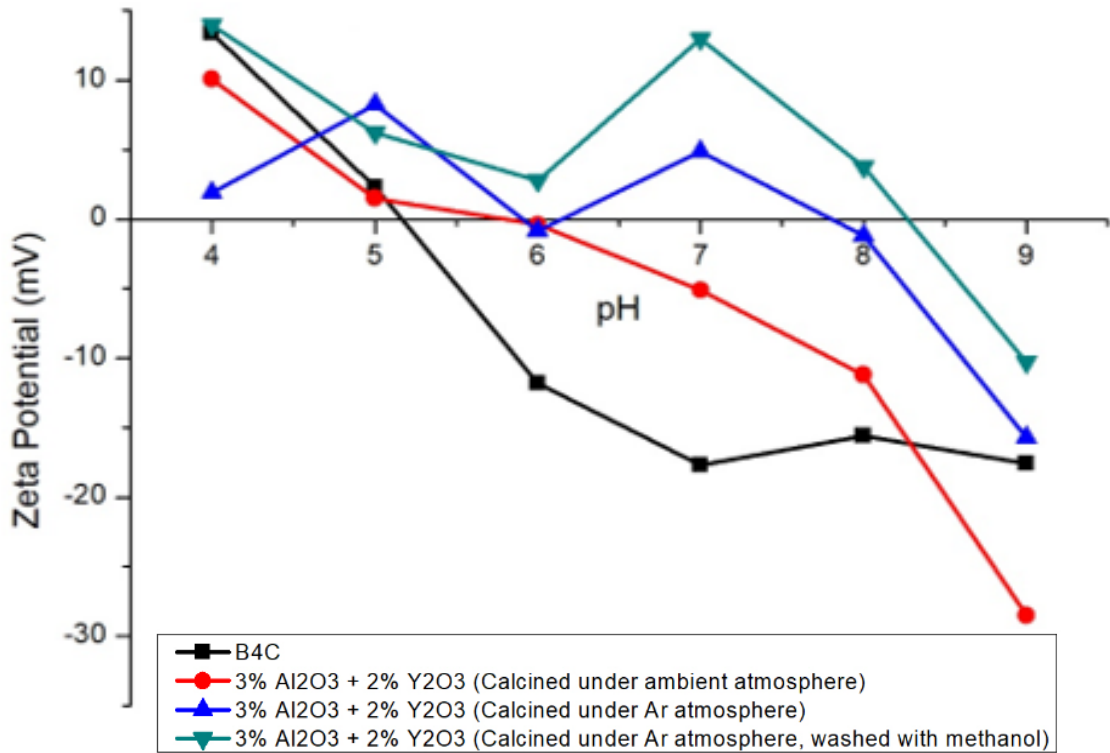


Figure 31. Zeta potential graph of the precipitated B₄C powders with the additives of 3% Al₂O₃ + 2% Y₂O₃ (Calcined under Ar atmosphere)

SEM images of back-scatter electron mode demonstrate the precipitated additives like the other prepared samples. Figure 32 shows the yttria as bright areas, alumina as semi-bright areas and boron carbide as dark areas. These images still shows the yttria agglomerations.

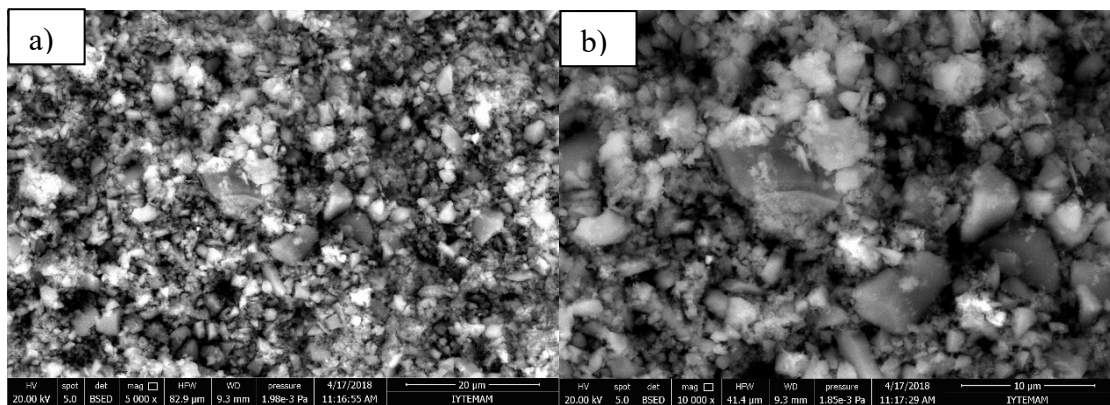


Figure 32. SEM (backscatter electron mode) image of the precipitated B₄C powders with the additives of 3% Al₂O₃ + 2% Y₂O₃ at a) low, b) high magnification (Calcined under Ar atmosphere)

4.2.4. Calcination Process under Protective Atmosphere

Another experiment is done to investigate the effect of the duration on the synthesized powders while the calcination temperature is increased to 500 °C. Figure 33 shows that all powders are taken from the same batch and calcined for 1-3-5 hours to compare the isoelectric points. While the powders calcined for 1 hour gave improved result with isoelectric point as 8,4 pH, other powders gave isoelectric point as 8,2 pH. They have almost same result because of the oxidation.

There is a big fluctuation at the samples calcined for 3 and 5 hours. The reason behind that can be the heterogeneous additive dispersion above the surface of boron carbide particles. Uneven dispersion and agglomeration of the yttria causes a fluctuation at the zeta potential graph, shows more than one intersection.

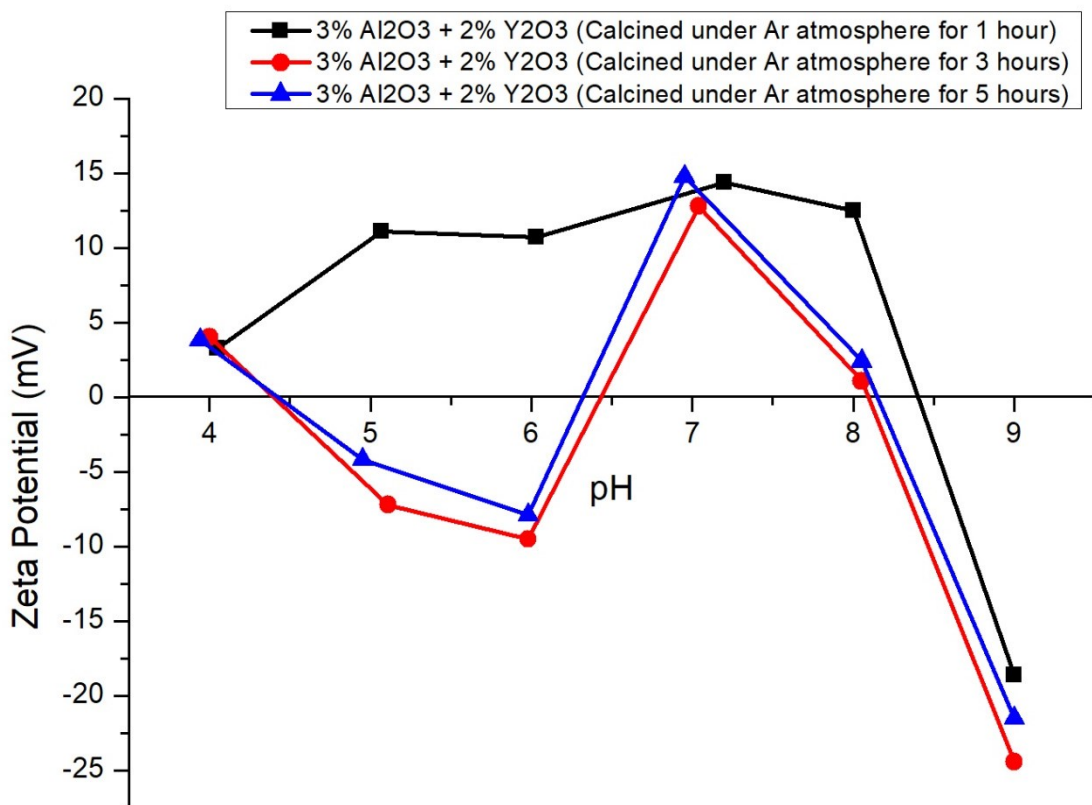


Figure 33. Zeta potential graph of the precipitated B₄C powders with the additives of 3% Al₂O₃ + 2% Y₂O₃ (Calcined under Ar atmosphere for 1-3-5 hours at 500 °C)

4.2.5. Ultrasonication Improvement for Optimized Precipitation

In order to compare the effects of different additive amounts, precipitation method is improved with the use of ultrasonic stirrer addition to the magnetic stirrer. Solution is mixed with ultrasonic stirrer for 15 minutes after the magnetic stirrer in order to eliminate the inadequate mixing possibility which can cause heterogeneous dispersion. Ultrasonic stirrer method uses micro scaled cavitation bubbles to restrain agglomeration of the additives during the precipitation but results are not successful as samples washed with methanol due to the oxide layer of the B₄C. Powders with the additives of 3% Al₂O₃ + 2% Y₂O₃ and 6% Al₂O₃ + 4% Y₂O₃ are analyzed and results are matches with each other. Methanol washed samples gave the true zeta potential results of the powders with isoelectric point as 8,5 pH in Figure 34. Powder with high additive as 6% Al₂O₃ + 4% Y₂O₃ gave the best result of the all experiments with smooth curve which is a sign of successful elimination of the oxide layer of B₄C.

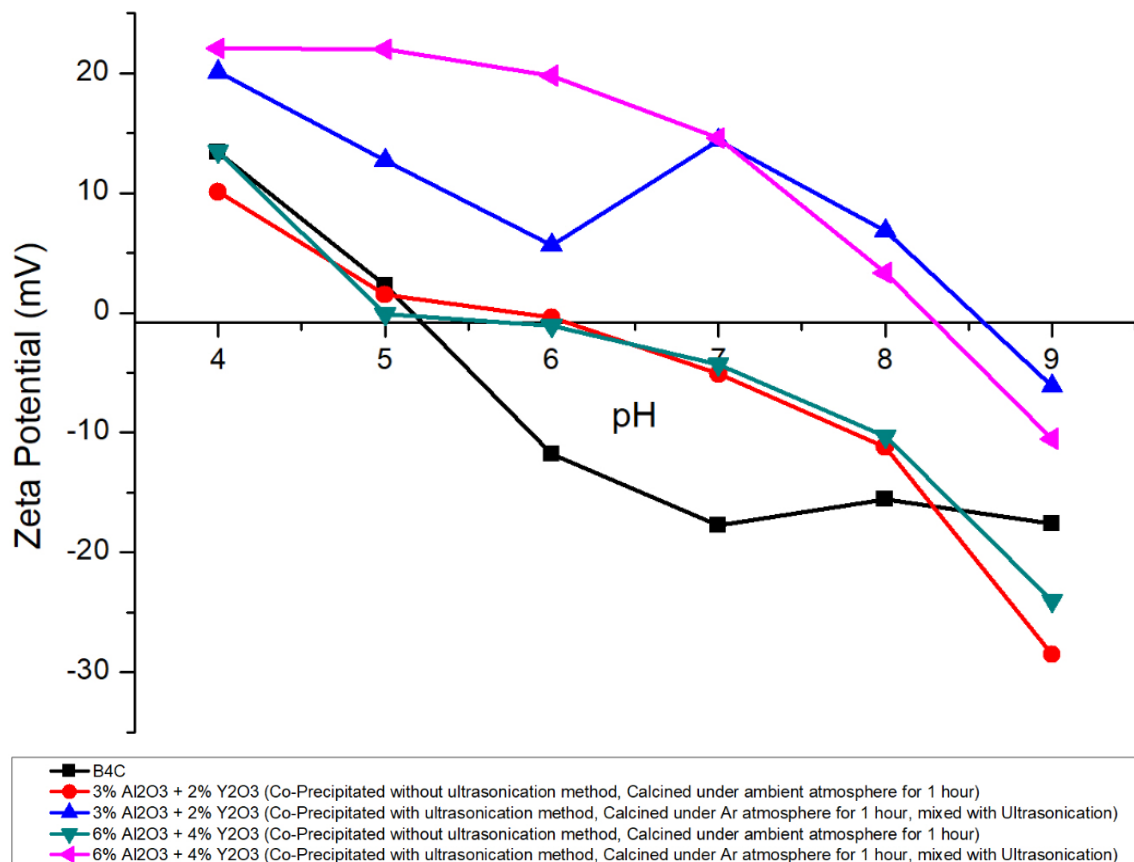


Figure 34. Zeta potential graph of the precipitated B₄C powders with the additives of 3% Al₂O₃ + 2% Y₂O₃ and 6% Al₂O₃ + 4% Y₂O₃ (Calcined under Ar atmosphere for 1 hour, mixed with ultrasonication method)

Figure 35 shows that there are yttria rich agglomerations at precipitated powders calcined for 5 hours. It is seen that when the precipitated powders are compared with the milled samples, additives of the precipitated powders are dispersed more homogeneously against the milled powders. It can be said that homogenization of additives is successful by the help of precipitation method. Layer of the additives are hard to detect at SEM images of precipitated powders. Particles size of the additives can be discovered as micron and sub-micron sized according to the SEM images of the milled samples.

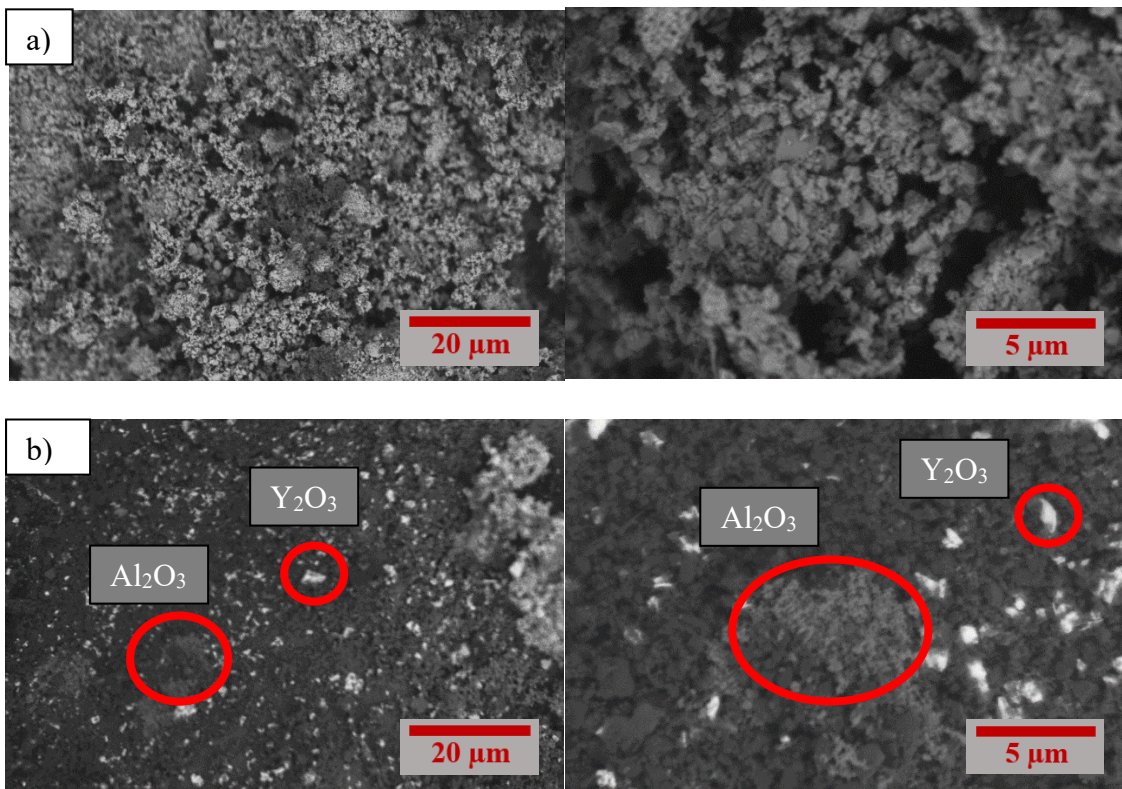


Figure 35. SEM (backscatter electron mode) image of the a) precipitated, b) milled B₄C Powders with the additives of 3% Al₂O₃ + 2% Y₂O₃

4.2.6. Comparison of the XRD Graphs of Powders

XRD graphs are scaled according to the peak at 24° and stacked for comparison in Figure 36. Graph below demonstrates the oxide peaks among the samples with different additive amounts. Even if the amounts of additives are different at three different samples, patterns are almost same at three of them. While there is also slight difference between the peaks at 38°, other peaks look same. Same XRD parameters are used for three

different experiments. Alumina and yttria peaks are not investigated at the XRD graphs due to the low coating thickness.

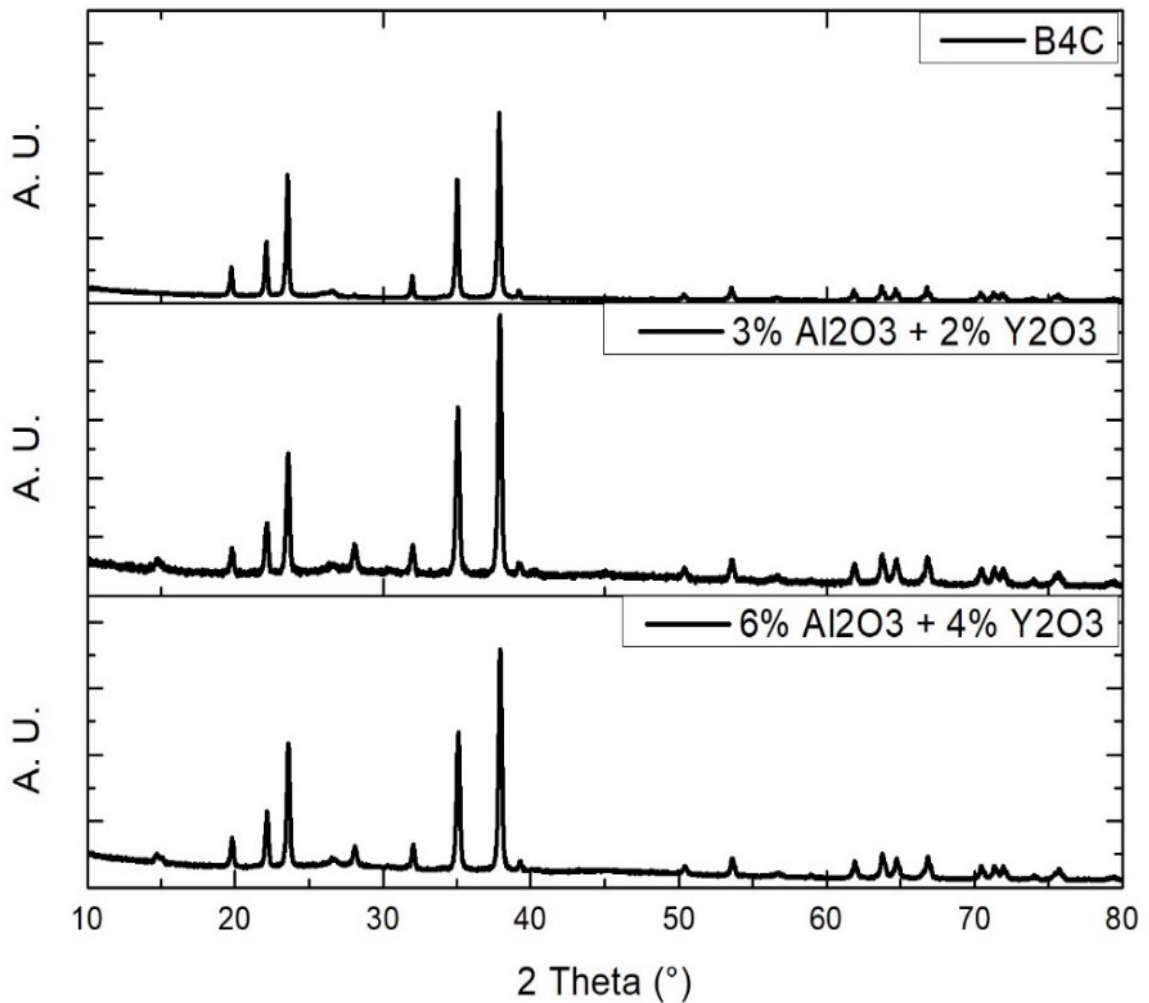


Figure 36. Stacked XRD graph of the precipitated B₄C powders with the additives of 3% Al₂O₃ + 2% Y₂O₃ and 6% Al₂O₃ + 4% Y₂O₃

Another comparison is done to investigate the improvements of the precipitated method below (see Figure 37). Oxide peaks are eliminated with the methanol washing and calcination under Ar atmosphere. Peak intensities at the 38° are also different like the graph above which is not expected because of the same additive amounts. Same XRD parameters are used for these experiments. Specific alumina and yttria peaks are not investigated at the graphs as before because of the low coating thickness of the additives as the previous XRD graphs. Existence of the additives are proven with the SEM images and EDS maps other than the XRD graphs.

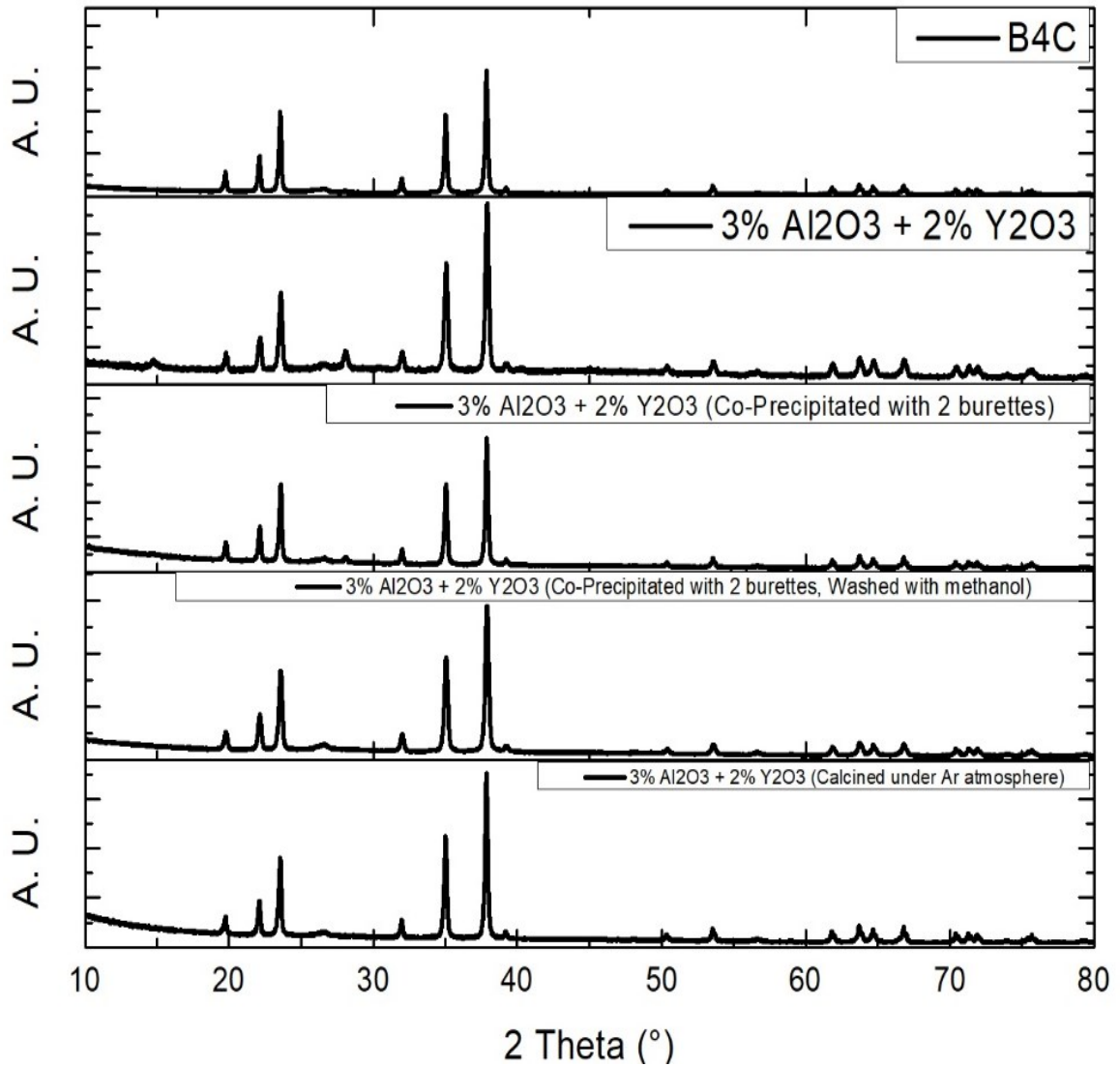


Figure 37. Stacked XRD graph of the precipitated B_4C powders with the additives of $3\% Al_2O_3 + 2\% Y_2O_3$

4.3. Sintering Studies

4.3.1. Effect of Precipitation Compared to Commercial Boron Carbide

Porosity of the sintered boron carbide sample is analyzed with ImageJ software and SEM image to give an idea of approximate result. Archimedes method is not applicable for the sintered compacts due to the stability of the sintered samples. Sintered compacts are easily getting went to pieces during the preparing stage. Sintering is done at $1750\text{ }^\circ\text{C}$ for 1 hour under Ar atmosphere.

As seen in Figure 38, BSED images shows the elemental analysis of the sintered compact with the help of backscattered electron mode of SEM. No material other than the B₄C is identified as bright area at the image which can be seen in an image.

As shown in Figure 39, ETD images show the morphology of the sintered structure with the help of secondary electron mode of SEM. Sharp B₄C particles are seen in the image with low amounts of necking between them. Low sintering temperature and low atmospheric pressure are the reasons for the low relative density.

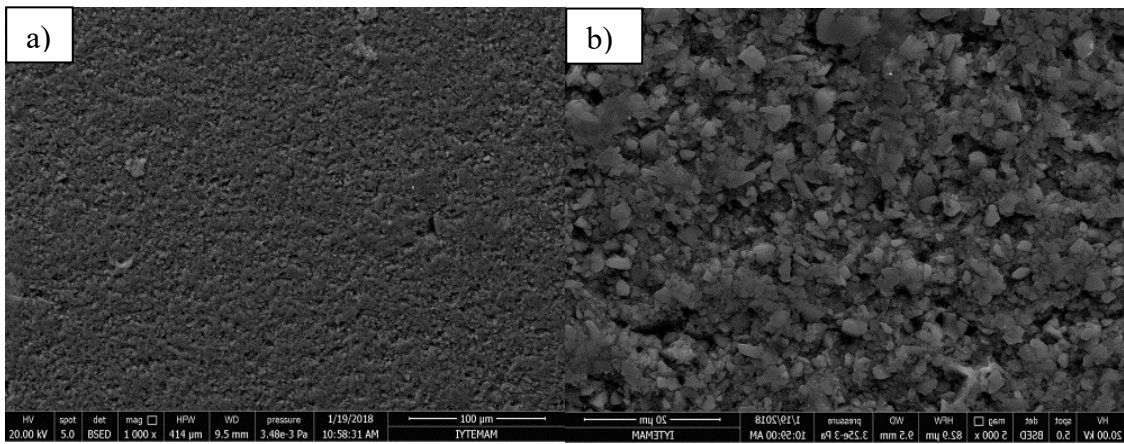


Figure 38. SEM (backscatter electron mode) image of the commercial B₄C compact at a) low, b) high magnification

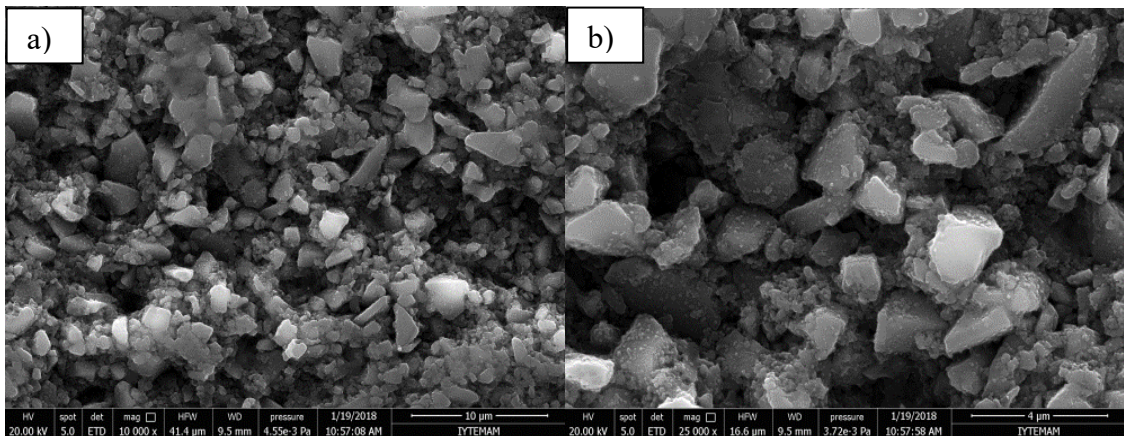


Figure 39. SEM (secondary electron mode) image of the commercial B₄C compact at a) low, b) high magnification

As seen in Figure 40 and 41, SEM images show that additives reduce the porosity with the help of additives. While the bright spots show the place of the yttria clusters, alumina is seen dispersed more homogeneous.

Figure 42 shows that porosity is lower than the commercial boron carbide compacts because of the increased necking between particles. Moreover, observable particles are seen rounded compared to the sharp commercial boron carbide powders. It can be said that the sintering is started at 1750 °C with the oxide additives.

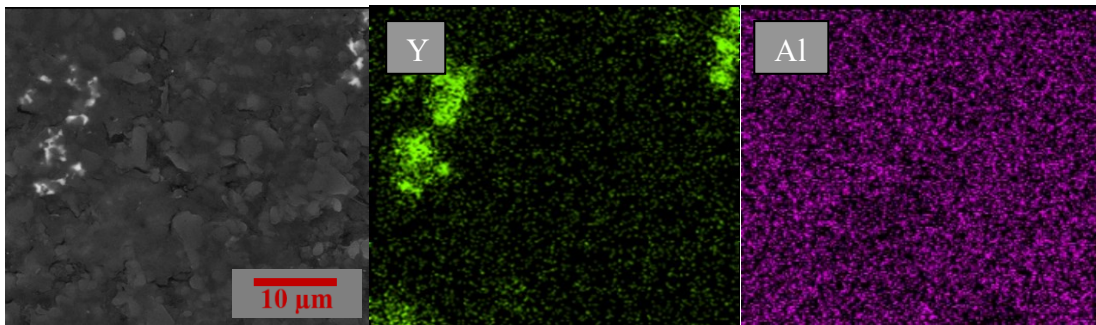


Figure 40. Elemental mapping images of the precipitated B₄C Powders with the Oxide Additives Calcined under Ambient Atmosphere

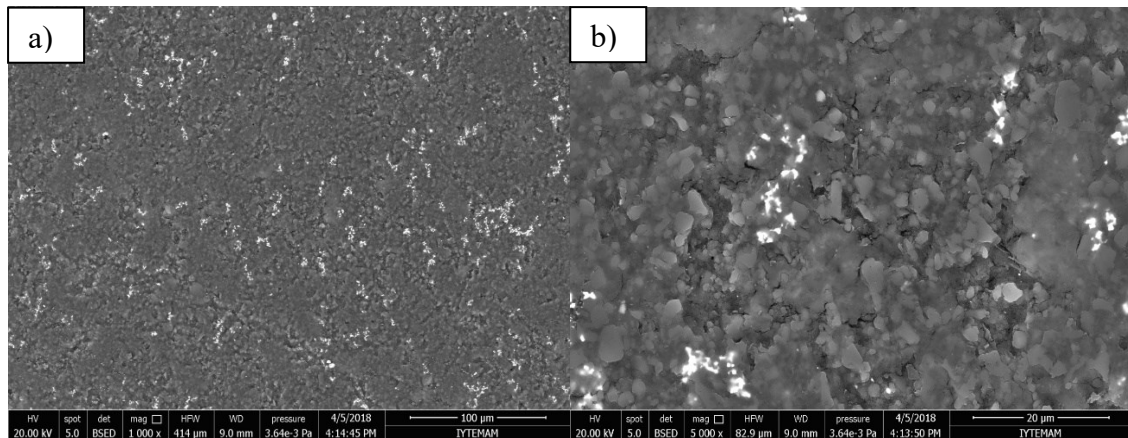


Figure 41. SEM (backscatter electron mode) image of the precipitated B₄C Powders with the Oxide Additives Calcined under Ambient Atmosphere at a) low, b) high magnification

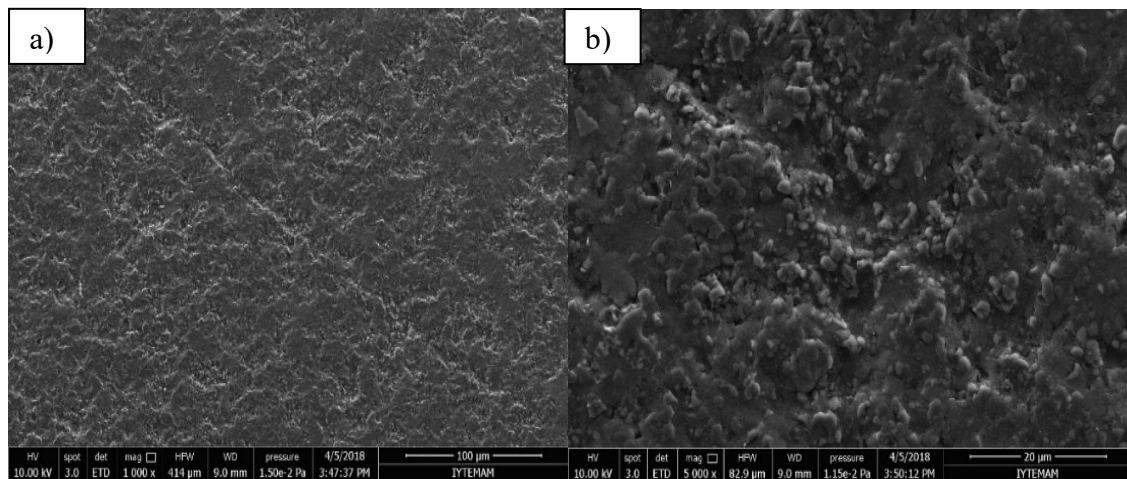


Figure 42. SEM (secondary electron mode) image of the precipitated B₄C Powders with the Oxide Additives Calcined under Ambient Atmosphere at a) low, b) high magnification

4.3.2. Effect of Calcination Time on Sintering

In order to advance the study, samples are sintered for different calcination time under Argon atmosphere to investigate the parameters like porosity of the sintered sample and the dispersion of the oxide additives. To eliminate residual material, calcination duration is limited to 1 hour for comparison.

BSED images shows the improved dispersion of the additives in Figure 43. Bright areas show the additive due to the higher atomic weight of the yttrium and aluminum which is not observed at the SEM image of the pure B₄C. In addition, elemental mapping of the BSED mode shows the dispersion of each elements which exhibits the oxide additives. While the aluminum is distributed more homogeneously, yttrium seems less homogeneous because of the high magnification in Figure 44.

ETD images of the sample clarifies the morphology and porosity of the compact in Figure 45. Necking occurred in the sintered compact more than the pure B₄C while the porosity is lower than that. Densification is improved with the sintering additives compared to the sintered compact of the commercial boron carbide powder. When the image taken with secondary electron mode compared to the image taken with backscatter electron mode, location of some bright particles matches at both images. These bright particles show the location of the yttria agglomerations.

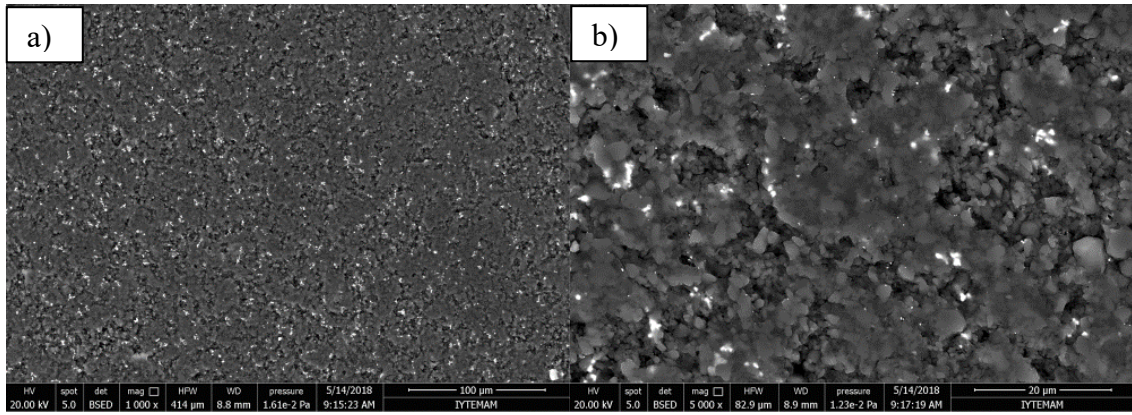


Figure 43. SEM (backscatter electron mode) image of the precipitated B₄C Powders with the Oxide Additives Calcined under Ar Atmosphere for 1 Hour at a) low, b) high magnification

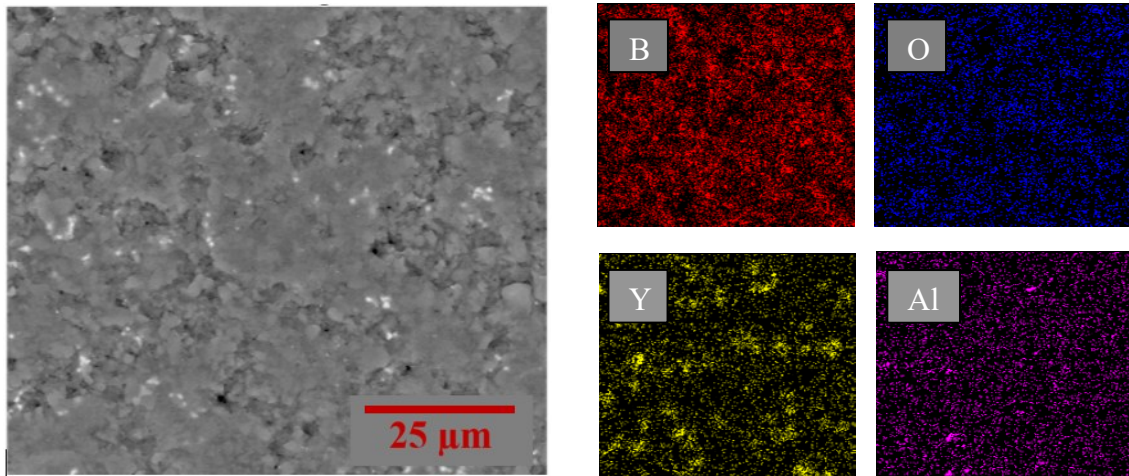


Figure 44. Elemental mapping images of the precipitated B₄C Powders with the Oxide Additives Calcined under Ar Atmosphere for 1 Hour

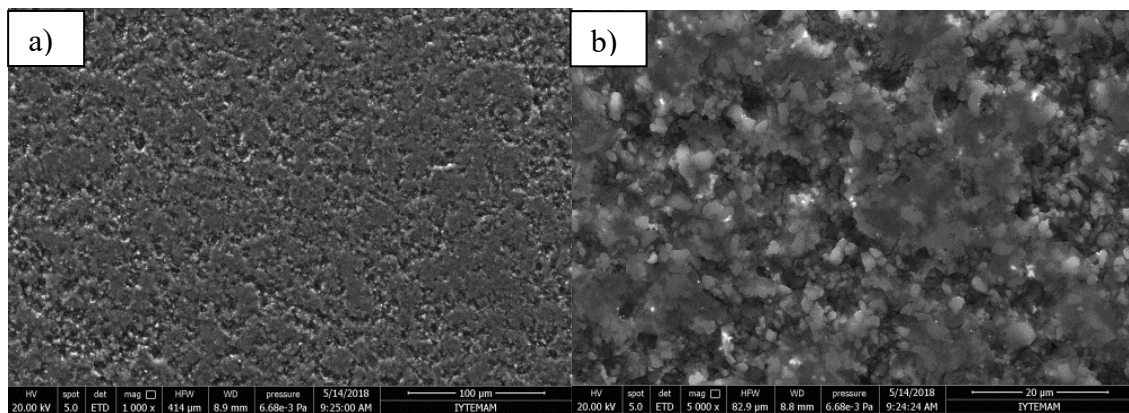


Figure 45. SEM (secondary electron mode) image of the precipitated B₄C Powders with the Oxide Additives Calcined under Ar Atmosphere for 1 Hour at a) low, b) high magnification

Calcination time is increased from 1 hour to 3 hours at this study. In order to successfully eliminate the residues left from precipitation, calcination time increased and its effect is observed. Most apparent effect is decreased porosity against pure B₄C and sample with 1 hour calcination.

As seen in Figure 46, BSED images also show successful dispersion of the oxide additives as a sample calcined for 3 hours. It can be also seen that the precipitated oxide additives are precipitated at the boundaries of the B₄C particles which improves the liquid phase sintering. Elemental mapping demonstrates the similar results as before in Figure 47. While the aluminum is distributed as optimum as possible, yttrium seems a bit agglomerated. ETD images at Figure 48 shows the same necking characteristics. These characteristics are not changed for samples of 1 hour and 3 hours calcined.

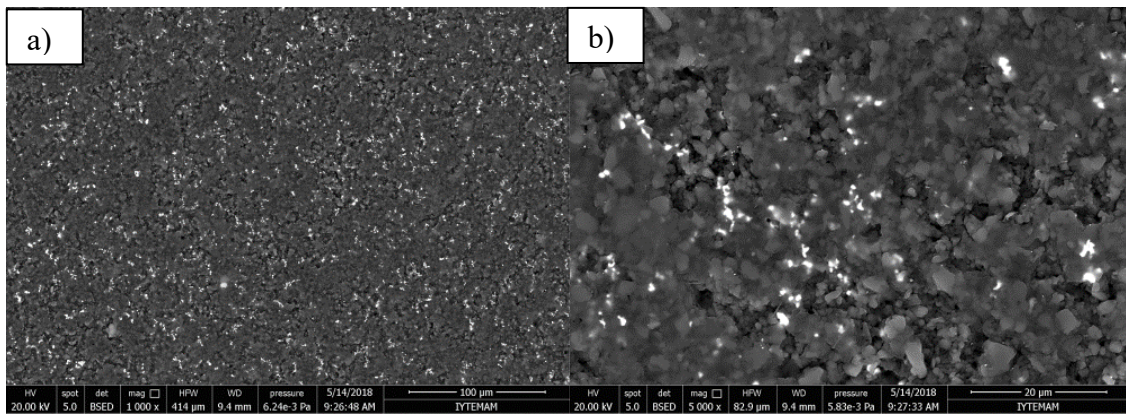


Figure 46. SEM (backscatter electron mode) image of the precipitated B₄C Powders with the Oxide Additives Calcined under Ar Atmosphere for 3 Hours at a) low, b) high magnification

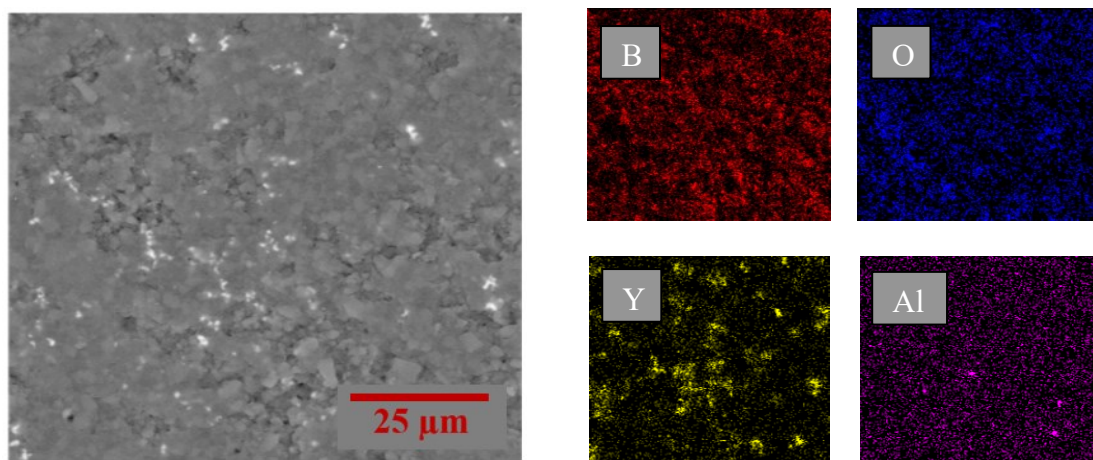


Figure 47. Elemental mapping images of the precipitated B₄C Powders with the Oxide Additives Calcined under Ar Atmosphere for 3 Hours

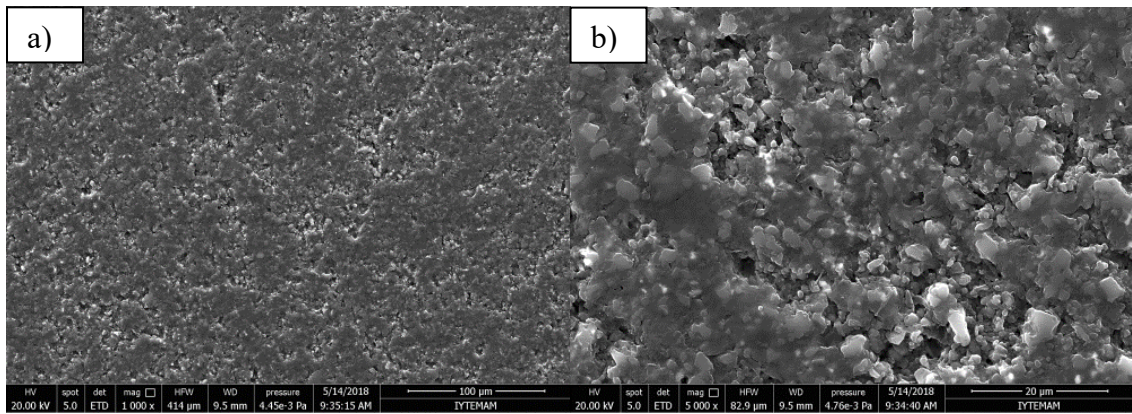


Figure 48. SEM (secondary electron mode) image of the precipitated B₄C Powders with the Oxide Additives Calcined under Ar Atmosphere for 3 Hours at a) low, b) high magnification

As seen in Figure 49, 50 and 51, BSED images, elemental mappings and ETD images show same distributions of the elements and same morphology as before. Dispersion of yttrium and aluminum is different from each other. While the aluminum is distributed more homogeneously, yttrium is distributed a bit agglomerated. This yttrium agglomeration reduces the chance of activating a liquid phase sintering. Due to these similar results of the samples calcined for 3 and 5 hours, further durations like 7 hours or more are not studied.

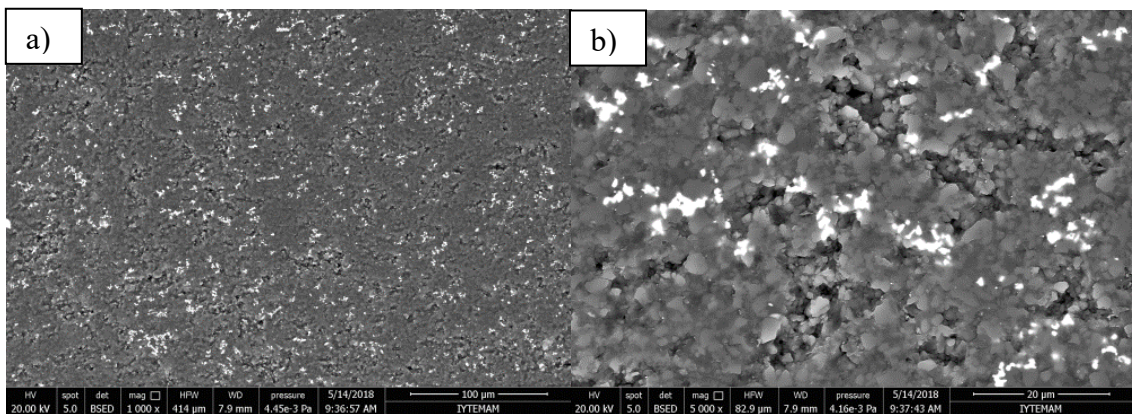


Figure 49. SEM (backscatter electron mode) image of the precipitated B₄C Powders with the Oxide Additives Calcined under Ar Atmosphere for 5 Hours at a) low, b) high magnification

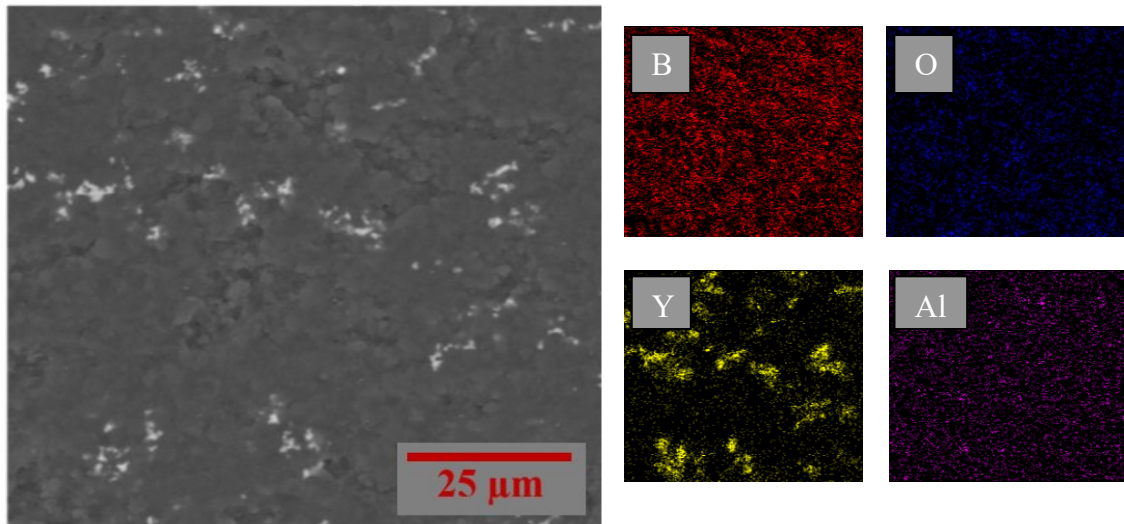


Figure 50. Elemental mapping images of the precipitated B₄C Powders with the Oxide Additives Calcined under Ar Atmosphere for 5 Hours

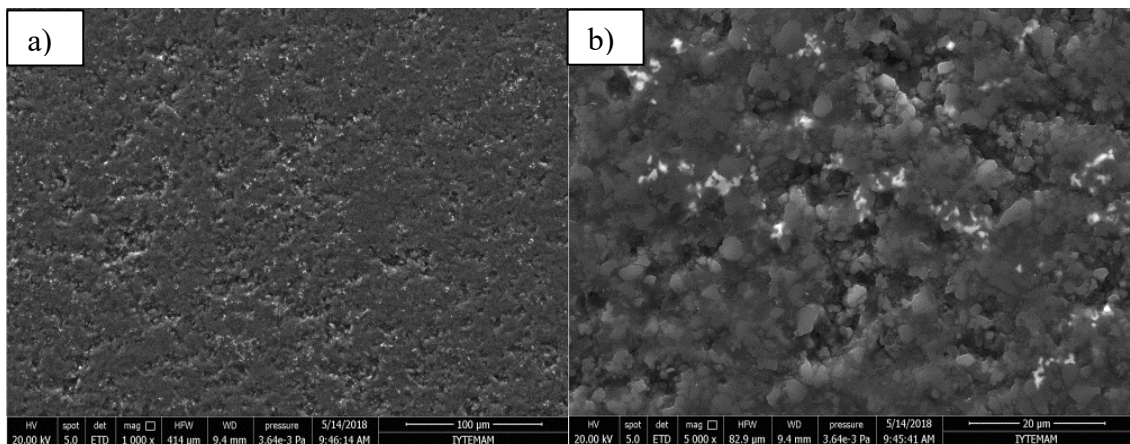


Figure 51. SEM (secondary electron mode) image of the precipitated B₄C Powders with the Oxide Additives Calcined under Ar Atmosphere for 5 Hours at a) low, b) high magnification

As shown in Figure 52, dispersion of the yttrium is compared between 1,3 and 5 hours of calcination duration. It is seen that the agglomeration is getting bigger when the calcination time increases to 5 hours which can be related to the oxidation of the B₄C.

In addition, another EDS analysis is also done to observe the result of B₄C powders with the additives of 3% Al₂O₃ + 2% Y₂O₃ at low magnification. It shows that the additive dispersion is homogeneous all over the images while the heterogeneous

dispersion is only observable at high magnifications like 5000x according to the former analyses (see Figure 53).

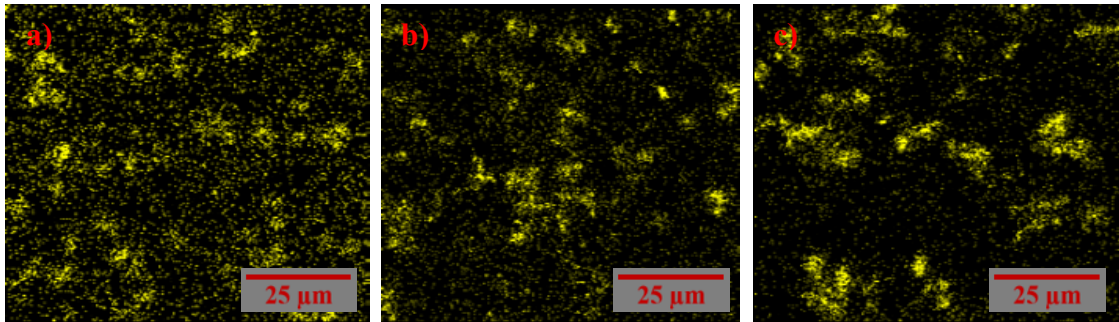


Figure 52. EDS maps of the yttrium in the precipitated and sintered B₄C powders with the additives of 3% Al₂O₃ + 2% Y₂O₃ (a) Calcined for 1 hour, b) Calcined for 3 hours, c) Calcined for 5 hours)

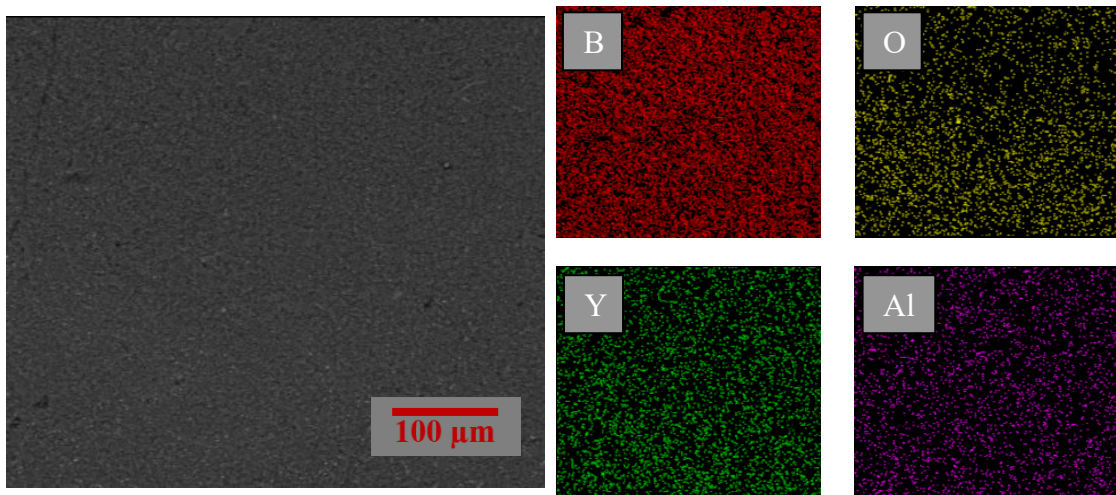


Figure 53. Elemental mapping images of the precipitated B₄C Powders with the Oxide Additives Calcined under Ar Atmosphere at 1000x magnification

Figure 54 shows the EDS analysis of precipitated and sintered B₄C powders with the additives of 3% Al₂O₃ + 2% Y₂O₃. Two different areas are taken into consideration for comparing the bright and dark areas. According to the EDS analysis of the sintered compact, high amount of yttrium is detected at the Spectrum 6 while the Spectrum 7 doesn't have yttrium peaks. On the other hand, amount of aluminum is almost 20% higher at the dark area. This analysis demonstrates that the dispersion of both additives is not evenly distributed while the aluminum is dispersed better. It is also seen that the precipitated and agglomerated yttrium additive is scaled up to 10 micrometers.

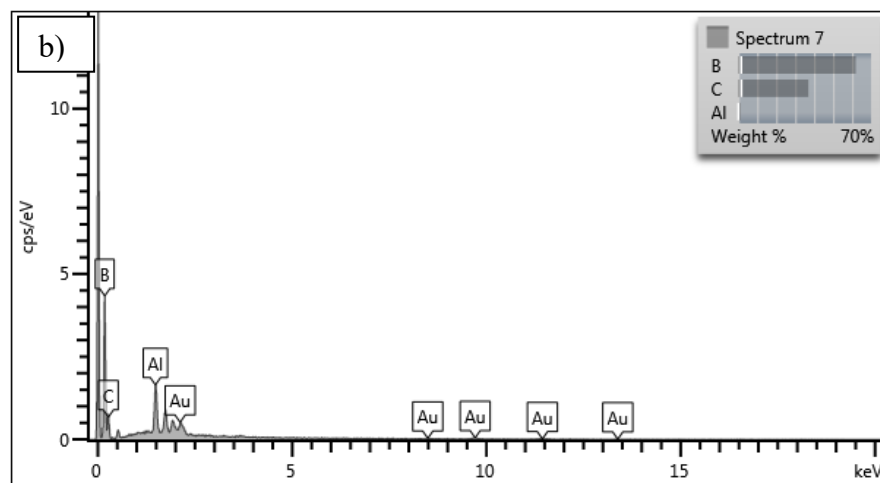
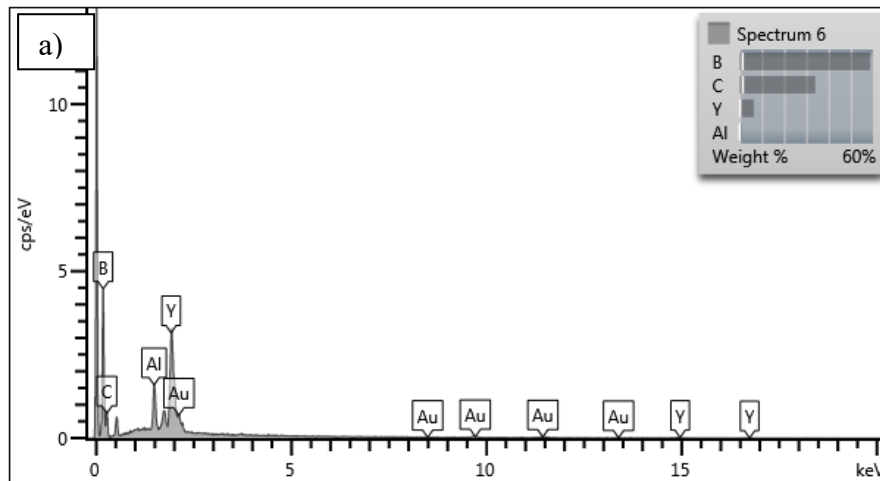
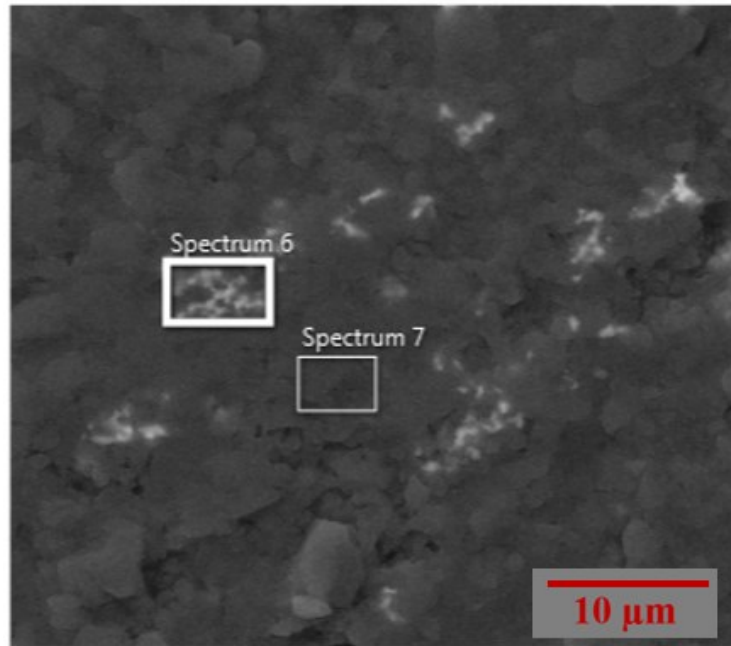


Figure 54. EDS graphs of the precipitated and sintered B₄C powders with the additives of 3% Al₂O₃ + 2% Y₂O₃, a) Spectrum 6, b) Spectrum 7

4.3.3. Sintered Sample of Milled Powders

In order to compare the benefits of the precipitation method, pure B_4C is mixed with the same amount of oxide additives which are equal to 3% Al_2O_3 and 2% Y_2O_3 of the whole mixture at the mill for 8 hours. Same sintering conditions as precipitated samples are applied for the milled powders for proper comparison.

BSED images show the yttrium at brightest areas while the aluminum is seen less bright in Figure 55. It is the fact that both yttrium and aluminum are seen agglomerated even at 1000x magnification. When the second image is examined at 10000x, cracks and pores are clearly seen and they are placed beside the yttrium particles. It can be concluded that the heterogeneous additive dispersion fails to start the liquid phase sintering and to fill the pores successfully.

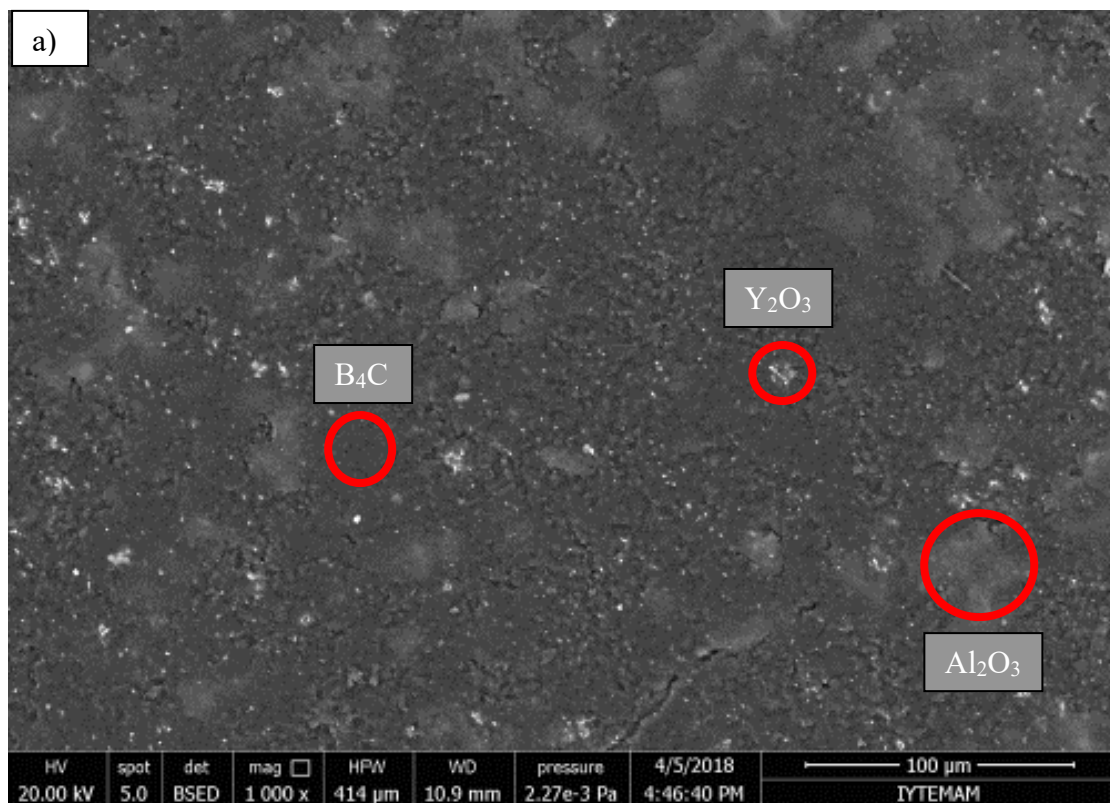


Figure 55. (Cont. on next page)

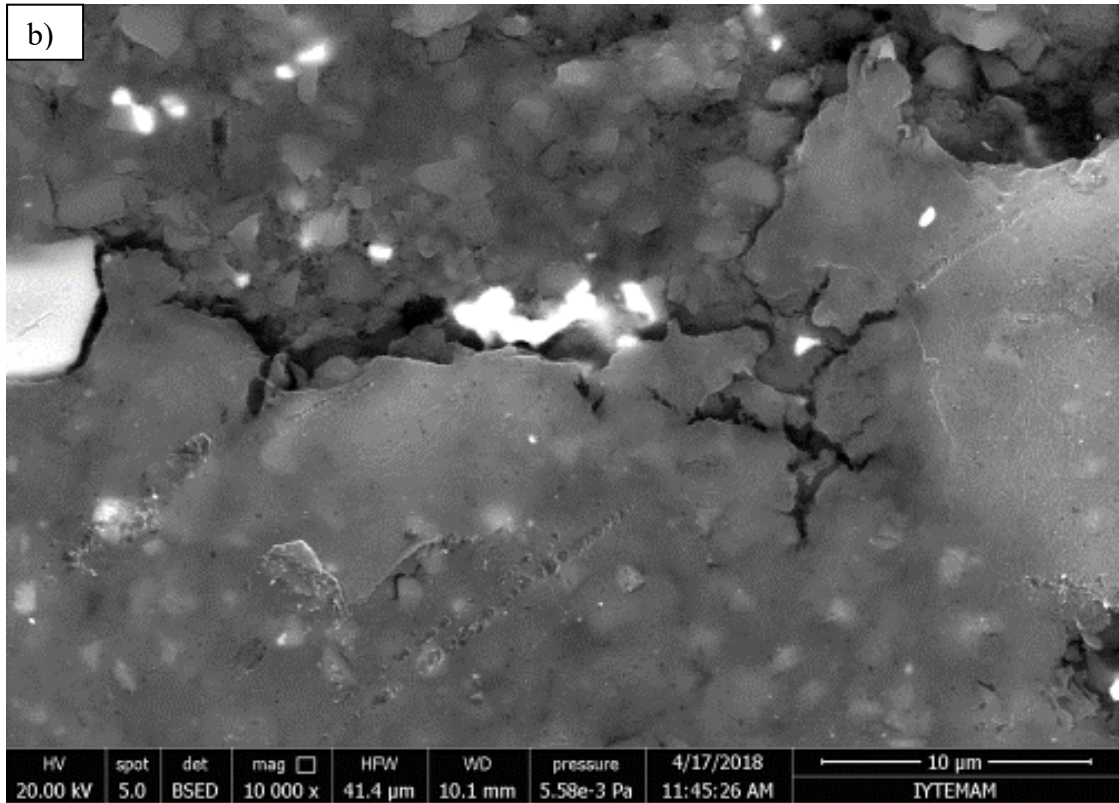


Figure 55. SEM (backscatter electron mode) images of the milled B₄C Powders with the Oxide Additives at a) low, b) high magnification (cont.)

As shown in Figure 56, yttrium and oxygen agglomeration is observed at the milled B₄C sample with oxide additives. It can be the reason of heterogeneous mixing during the milling process. Particles of the oxide additives are not dispersed as precipitated samples because precipitation process includes coating of the B₄C powders while the oxide particles are distributed separately at the milling process.

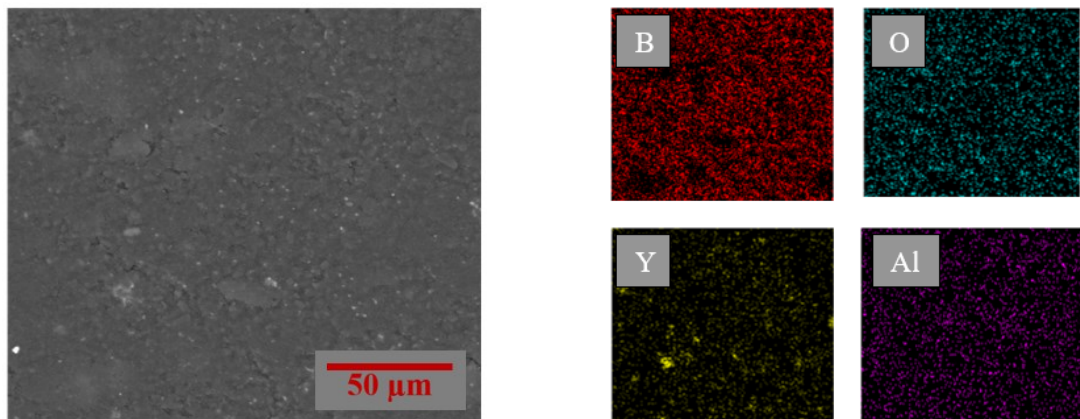


Figure 56. Elemental mapping images of the milled B₄C Powders with the Oxide Additives at 2500x magnification

When densities of the sintered compacts are compared with ImageJ analyses, precipitation method gives the best result against the commercial boron carbide and milled boron carbide powders with oxide additives (see Table 2). The reason is that additives are dispersed more homogeneously with the precipitation method which leads to better liquid phase sintering between the particles.

Table 2. Comparison of the porosities of commercial, milled and precipitated boron carbide powders

Powder Type	Commercial Boron Carbide Compact	Milled Boron Carbide Compact	Precipitated Boron Carbide Compact
Porosity	16,10 %	17 %	12,44 %

CHAPTER 5

CONCLUSIONS

Precipitation method is used as an addition method of sintering additives in this study. Both the nitrate salts of the additives and the boron carbide powder have been mixed in the water while the ammonia solution is used as a pH equalizer. After aging and drying stages of the solution, agglomerated powders are crushed with mortar and calcined in a tube furnace. As a result of these processes, boron carbide powders are coated with the oxide additives. Below conclusions are obtained as a result of this study.

- Boron carbide powders are prone to oxidize in an ambient atmosphere. Even the raw boron carbide powders have an oxide peak at the XRD graph. Methanol washing is a proper method to eliminate the oxide layer above the surface of the boron carbide powders. Methanol washing moves the isoelectric point of the boron carbide from 5.2 pH to 4.7 pH in a zeta potential graph.
- Most of the precipitation in this study is done with one burette while the second burette is used for ammonia solution. Separating the oxide additives to two burette does not change the surface characteristics of the precipitated powder according to the zeta potential graph.
- Calcination atmosphere is important for the oxidation of boron carbide powders. Changing the atmosphere from ambient to Argon changes the oxidation behavior of the boron carbide powders due to the lack of oxygen. There are no oxide peaks at the XRD graph of the 3% Al₂O₃ + 2% Y₂O₃ and isoelectric point moves from 6 pH to 8 pH with the Argon atmosphere. Methanol washing also translates the isoelectric point further to 8.3 pH.
- Effect of the calcination is also investigated and it is found that formation of oxide layer is occurred according to the zeta potential graph. When the calcination time increases from 1 to 3 and 5, isoelectric point and trend of the graph changes. There is a slight peak between 5 to 6 pH which is a sign of oxide layer above the surface of the boron carbide powders. It is also seen that when the zeta potential solutions are ultrasonicated with methanol for eliminating oxide layer, 3 hours calcined sample loses the oxide peak while the 5 hours calcined sample stays almost same.

Ultrasonication with methanol eliminates the oxide layer and increases the isoelectric point.

- When the calcined samples sintered, it is seen that long-time calcined samples like 3 and 5 hours have lower porosity than 1 hour calcined sample but yttrium oxide dispersion is getting more heterogeneous as a result of increased calcination time. Oxide formation can be the reason behind this consequence.
- Porosity and agglomeration of yttria and alumina are increased at the sintered samples of milled powders when the SEM images are compared with precipitated samples. The reason behind that is heterogeneous dispersion of the oxide additives at the milling process compared to the coating stage of the precipitation.

REFERENCES

- [1] Thévenot, F. (1990). Boron carbide—A comprehensive review. *Journal of the European Ceramic Society*, 6(4), 205-225. doi:10.1016/0955-2219(90)90048-k
- [2] Suri, A. K., Subramanian, C., Sonber, J. K., & Murthy, T. S. (2010). Synthesis and consolidation of boron carbide: A review. *International Materials Reviews*, 55(1), 4-40. doi:10.1179/095066009x12506721665211
- [3] Shupe, J. (2009). *Densification of nano-sized boron carbide* (Unpublished master's thesis). Georgia Institute of Technology.
- [4] Mashhadi, M., Taheri-Nassaj, E., & Sglavo, V. M. (2010). Pressureless sintering of boron carbide. *Ceramics International*, 36(1), 151-159. doi:10.1016/j.ceramint.2009.07.034
- [5] Lee, H., & Speyer, R. F. (2003). Pressureless Sintering of Boron Carbide. *Journal of the American Ceramic Society*, 86(9), 1468-1473. doi:10.1111/j.1151-2916.2003.tb03498.x
- [6] Lippmann, H., & Iankov, R. (1997). Mathematical modeling of sintering during powder forming processes. *International Journal of Mechanical Sciences*, 39(5), 585-596. doi:10.1016/s0020-7403(96)00062-8
- [7] Lee, H., & Speyer, R. F. (2003). Pressureless Sintering of Boron Carbide. *Journal of the American Ceramic Society*, 86(9), 1468-1473. doi:10.1111/j.1151-2916.2003.tb03498.x
- [8] Roy, T., Subramanian, C., & Suri, A. (2006). Pressureless sintering of boron carbide. *Ceramics International*, 32(3), 227-233. doi:10.1016/j.ceramint.2005.02.008

- [9] Kim, H., Koh, Y., & Kim, H. (2004). Densification and Mechanical Properties of B4C with Al₂O₃ as a Sintering Aid. *Journal of the American Ceramic Society*, 83(11), 2863-2865. doi:10.1111/j.1151-2916.2000.tb01647.x
- [10] Dobrzanski, L. A., Dobrzanska-Danikiewicz, A. D., Achtelik-Franczak, A., Dobrzanski, L. B., Hajduczek, E., & Matula, G. (2017). Fabrication Technologies of the Sintered Materials Including Materials for Medical and Dental Application. *Powder Metallurgy - Fundamentals and Case Studies*. doi:10.5772/65376
- [11] Yushin, D. I., Smirnov, A. V., Pinargote, N. W., Peretyagin, P. Y., & Millan, R. T. (2015). Modeling Process of Spark Plasma Sintering of Powder Materials by Finite Element Method. *Materials Science Forum*, 834, 41-50. doi:10.4028/www.scientific.net/msf.834.41
- [12] Bogomol, I., Grasso, S., Nishimura, T., Sakka, Y., Loboda, P., & Vasylykiv, O. (2012). Hard polycrystalline eutectic composite prepared by spark plasma sintering. *Ceramics International*, 38(5), 3947-3953. doi:10.1016/j.ceramint.2012.01.048
- [13] Tanaka, H., Yamamoto, A., Shimoyama, J., Ogino, H., & Kishio, K. (2012). Strongly connected *ex situ* MgB₂ polycrystalline bulks fabricated by solid-state self-sintering. *Superconductor Science and Technology*, 25(11), 115022. doi:10.1088/0953-2048/25/11/115022
- [14] German, R. M. (2014). *Liquid Phase Sintering*. Springer Verlag.
- [15] German, R. M., Suri, P., & Park, S. J. (2009). Review: Liquid phase sintering. *Journal of Materials Science*, 44, 1-39. doi:10.1007/s10853-008-3008-0
- [16] Dole, S. L., Prochazka, S., & Doremus, R. H. (1989). ChemInform Abstract: Microstructural Coarsening During Sintering of Boron Carbide. *ChemInform*, 20(43). doi:10.1002/chin.198943288
- [17] Yin, B., & Wang, L. (2003). Studies on activated sintering of jet milled B4C powders. *Atomic Energy Science and Technology*, 37, 70-72.

- [18] Baharvandi, H., & Hadian, A. (2007). Pressureless Sintering of TiB₂-B₄C Ceramic Matrix Composite. *Journal of Materials Engineering and Performance*, 17(6), 838-841. doi:10.1007/s11665-007-9182-4
- [19] Subramanian, C., Roy, T., Murthy, T., Sengupta, P., Kale, G., Krishnaiah, M., & Suri, A. (2008). Effect of zirconia addition on pressureless sintering of boron carbide. *Ceramics International*, 34(6), 1543-1549. doi:10.1016/j.ceramint.2007.04.017
- [20] Baharvandi, H. R., Hadian, A. M., Abdizadeh, A., & Ehsani, N. (2006). Investigation on addition of ZrO₂-3 mol% Y₂O₃ powder on sintering behavior and mechanical properties of B₄C. *Journal of Materials Science*, 41(16), 5269-5272. doi:10.1007/s10853-006-0355-6
- [21] Levin, L., Frage, N., & Dariel, M. P. (1999). The effect of Ti and TiO₂ additions on the pressureless sintering of B₄C. *Metallurgical and Materials Transactions A*, 30(12), 3201-3210. doi:10.1007/s11661-999-0230-6
- [22] Levin, L., Frage, N., & Dariel, M. (2000). A novel approach for the preparation of B₄C-based cermets. *International Journal of Refractory Metals and Hard Materials*, 18(2-3), 131-135. doi:10.1016/s0263-4368(00)00012-3
- [23] Lee, C. H., & Kim, C. H. (1992). Pressureless sintering and related reaction phenomena of Al₂O₃-doped B₄C. *Journal of Materials Science*, 27(23), 6335-6340. doi:10.1007/bf00576282
- [24] Sigl, L. (1998). Processing and mechanical properties of boron carbide sintered with TiC. *Journal of the European Ceramic Society*, 18(11), 1521-1529. doi:10.1016/s0955-2219(98)00071-5
- [25] Li, X., Jiang, D., Zhang, J., Lin, Q., Chen, Z., & Huang, Z. (2014). Pressureless sintering of boron carbide with Cr₃C₂ as sintering additive. *Journal of the European Ceramic Society*, 34(5), 1073-1081. doi:10.1016/j.jeurceramsoc.2013.11.036

- [26] Wei, R., Zhang, Y., Gong, H., Jiang, Y., & Zhang, Y. (2013). The effects of rare-earth oxide additives on the densification of pressureless sintering B₄C ceramics. *Ceramics International*, 39(6), 6449-6452. doi:10.1016/j.ceramint.2013.01.073
- [27] Goldstein, A., Yeshurun, Y., & Goldenberg, A. (2007). B₄C/metal boride composites derived from B₄C/metal oxide mixtures. *Journal of the European Ceramic Society*, 27(2-3), 695-700. doi:10.1016/j.jeurceramsoc.2006.04.042
- [28] Miyazaki, H., Zhou, Y., Hyuga, H., Yoshizawa, Y., & Kumazawa, T. (2010). Microstructure of boron carbide pressureless sintered in an Ar atmosphere containing gaseous metal species. *Journal of the European Ceramic Society*, 30(4), 999-1005. doi:10.1016/j.jeurceramsoc.2009.10.015
- [29] Goldstein, A., Geffen, Y., & Goldenberg, A. (2001). Boron Carbide-Zirconium Boride In Situ Composites by the Reactive Pressureless Sintering of Boron Carbide-Zirconia Mixtures. *Journal of the American Ceramic Society*, 84(3), 642-644. doi:10.1111/j.1151-2916.2001.tb00714.x
- [30] Yang, J., Ohji, T., & Niihara, K. (2004). Influence of Yttria-Alumina Content on Sintering Behavior and Microstructure of Silicon Nitride Ceramics. *Journal of the American Ceramic Society*, 83(8), 2094-2096. doi:10.1111/j.1151-2916.2000.tb01520.x
- [31] Sun, E. Y., Becher, P. F., Plucknett, K. P., Hsueh, C., Alexander, K. B., Waters, S. B., . . . Brito, M. E. (2005). Microstructural Design of Silicon Nitride with Improved Fracture Toughness: II, Effects of Yttria and Alumina Additives. *Journal of the American Ceramic Society*, 81(11), 2831-2840. doi:10.1111/j.1151-2916.1998.tb02703.x
- [32] Winn, E. J., & Clegg, W. J. (2004). Role of the Powder Bed in the Densification of Silicon Carbide Sintered with Yttria and Alumina Additives. *Journal of the American Ceramic Society*, 82(12), 3466-3470. doi:10.1111/j.1151-2916.1999.tb02266.x
- [33] Fabrichnaya, O., Pavlyuchkov, D., Neher, R., Herrmann, M., & Seifert, H. (2013). Liquid phase formation in the system Al₂O₃-Y₂O₃-AlN: Part II. Thermodynamic

assessment. *Journal of the European Ceramic Society*, 33(13-14), 2457-2463.
doi:10.1016/j.jeurceramsoc.2013.05.004

[34] Iturriza, I., Castro, F., & Fuentes, M. (1989). Sinter and sinter-HIP of silicon nitride ceramics with yttria and alumina additions. *Journal of Materials Science*, 24(6), 2047-2056. doi:10.1007/bf02385420

[35] Toropov, N. A., Bondar, I. A., Galadhov, F. Y., Nikogosyan, K. S., & Vinogradova, N. V. (1964). Phase equilibria in the yttrium oxide-alumina system. *Bulletin of the Academy of Sciences, USSR Division of Chemical Science*, 13(7), 1076-1081. doi:10.1007/bf00863104

[36] Precipitation and Co-precipitation. (n.d.). Lecture. Retrieved July 11, 2018, from <http://nptel.ac.in/courses/103103026/7>

[37] Halverson, D. C., Pyzik, A. J., Aksay, I. A. and Snowden, W. E. (1989), Processing of Boron Carbide-Aluminum Composites. *Journal of the American Ceramic Society*, 72: 775-780. doi:10.1111/j.1151-2916.1989.tb06216.x

[38] “Zetasizer Nano ZS.” Zeta Potential. Accessed November 5, 2019. <https://www.malvernpanalytical.com/en/products/product-range/zetasizer-range/zetasizer-nano-range/zetasizer-nano-zs>.

[39] “İzmir Yüksek Teknoloji Enstitüsü.” Malzeme Araştırma Merkezi. Accessed November 5, 2019. <https://mam.iyte.edu.tr/>.